

Foundation for Research and Technology – Hellas
Institute of Applied and Computational Mathematics

EDELWEIS 2014
Localization Analysis

E.K. Skarsoulis and G.S. Piperakis

25 November 2014

Contents

1. Introduction

2. The localization method

3. Experimental data and pre-processing

3.1 The Edelweis'14 controlled localization experiment

3.1.1 Preliminary propagation calculations

3.1.2 Experiment implementation

3.1.3 Shortcomings

3.2 Position data

3.2.1 GPS data (ship and AOBs)

3.2.2 TDR data (source depth)

3.2.3 Estimated source-receiver ranges

3.2.4 Hydrophone depths

3.3 Travel-time data

3.3.1 Raw data

3.3.2 Pre-processing (filtering + energy filter)

3.3.3 Differential travel times between direct and surface-reflected arrivals

3.3.4 Differential travel times between direct arrivals at AOB1 and AOB2 – synchronization problem

3.4 Measured sound-speed profile

3.5 Model-based synchronization – offset calibration

4. Localization results

4.1 Comparison of isochrones with range-depth verification data

4.2 Source range and depth estimation – effect of hydrophone depth uncertainty

4.3 Inversion of TOAD data using source-depth constraint

5. Discussion and Conclusions

6. References

Appendix A. Localization with shallow hydrophones

1. Introduction

In 1998 an important resident population of sperm whales was discovered in the Greek Seas by Alexandros Frantzis and his group at the Pelagos Cetacean Research Institute [1,2]. Subsequent research carried out by Pelagos revealed that the Hellenic Trench constitutes a critical habitat for sperm whales not only locally, but also at the regional level [3,4]. In 2002 the Parties of ACCOBAMS recognized the offshore waters of SW Crete as a key area for the conservation of Mediterranean sperm whales. In 2007 the 20 countries members of ACCOBAMS included the Hellenic Trench in the official map of the areas that urgently need to be assigned the status of Marine Protected Areas for cetaceans. In addition, in 2006 a Red List assessment conducted jointly by IUCN and ACCOBAMS concluded that the Mediterranean sperm whale population qualifies as “Endangered” under the IUCN Red List criteria [5].

The sperm-whale population that inhabits or crosses the Hellenic Trench is estimated to count ~200 individuals, and may represent the entire eastern Mediterranean population unit. Therefore these animals constitute a very vulnerable piece of the European wildlife. However, a significant number of them are dying because of collisions with large vessels, which is the most important threat locally [6]. On average, one sperm whale reaches the Greek coasts dead yearly, while having signs of collision with a large vessel. This number represents only a fraction of the whales that die after a collision, since other carcasses sink in offshore waters and are never seen. The high death rate due to collisions is obviously unsustainable and underlines the necessity to drastically mitigate this threat in a critical habitat.

A possible solution to this problem is to set up a listening/notification network of acoustic listening stations that will detect and localize sperm whales from the pulsed sounds (clicks) that they produce. The automatic detection and localization will be followed by a notification of large vessels in the broader area, such that they can reduce the probability of collision by slightly changing their course. The Edelweis’14 experiment was an initial step, a preliminary feasibility study in that direction, undertaken by CINTAL, FORTH, Pelagos and Univ. Basel and kindly supported by OceanCare. It took place in the Ionian Sea from 3-11 August 2014 and its objectives were to acquire acoustic data transmitted from an acoustic source deployed at depths compatible with sperm whale diving, in various configurations and setups so as to allow acoustic localization and validation, to acquire concurrent environmental data sufficient for propagation modeling, and finally, if possible, to obtain actual sperm whale vocalizations and use them for animal localization.

The first two objectives (controlled localization experiment and environmental data collection) were accomplished. The last objective was not met due to lack of sperm whale encounters. The data collected during the Edelweis’14 experiment were presented in detail in the Edelweis’14 Data Report [7]. The present report focuses on the analysis of the controlled localization experiment which was conducted on 9 August 2014 in deep waters (~1000 m water depth) southeast of the Zakynthos island in the Ionian Sea. Two buoys (Acoustic Oceanographic Buoys – AOBs) [8] with suspended vertical hydrophone arrays were deployed at nearby locations while an acoustic source was suspended from a ship (R/V Nereis) using a 600-1000-m long cable at various locations around the AOBs up to distances of ~4 km. The localization method exploits time of arrival differences (TOADs) between direct, and also between direct and surface-reflected arrivals at two hydrophones to obtain estimates for source range, depth and azimuth [9]. For the estimation of source range and depth it is not required to know the horizontal location of

the hydrophones but merely the hydrophone depths. If in addition the horizontal location of the two hydrophones is known then the source bearing can be estimated as well.

The contents of this report are organized as follows. In section 2 the localization method is described. Section 3 presents the experimental data obtained during the controlled localization experiment. The basic data sets are position data (ship and AOB GPS data, as well as source and hydrophone depth data), acoustic data (acoustic receptions of source signals at the suspended hydrophones) and environmental data (temperature, salinity and sound-speed profiles). While the initial plan was to collect GPS and source depth data for verification purposes, part of these data was used for offset calibration of the two buoys, because of lack of a common time reference (synchronization) of the two AOBs. In Section 4 the localization problem is addressed. A serious problem for the localization analysis is the lack of data for hydrophone depths. In this connection, a further part of the position data, the data for the source depth in particular, was used as an additional body of information to constrain the localization. In Section 5 the analysis results are discussed and conclusions are drawn.

2. The localization method

Two-hydrophone configurations with relatively short separations have been broadly used for bearing estimation of click producing animals, such as sperm whales. This is done by measuring relative travel times of direct arrivals at the two hydrophones and using the known hydrophone distance [10–12]. More recently two-hydrophone configurations with larger separations have been used for range and depth estimation of impulsive sources by exploiting both direct and surface-reflected arrivals (see 2.1), i.e. three differential travel times. In order to estimate range and depth in this case it is not required to know the distance between the hydrophones but merely the hydrophone depths [9,13]. If in addition the horizontal hydrophone location is known then the source bearing can be estimated as well, subject to left-right ambiguity.

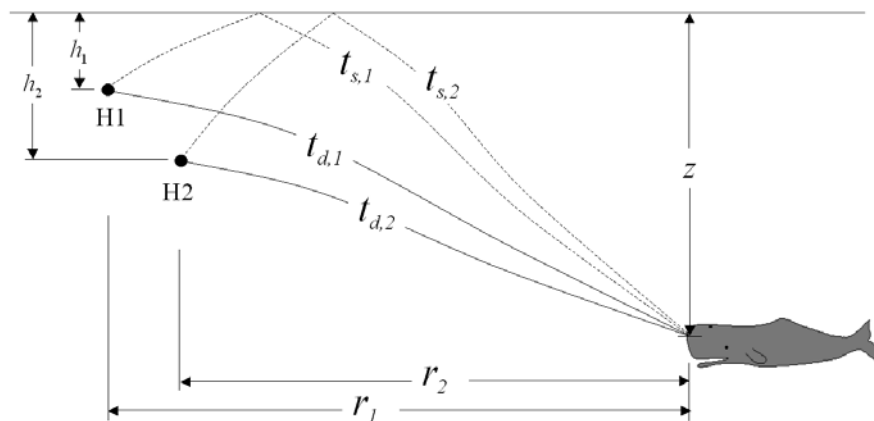


Fig. 2.1 Localization (range/depth estimation) of an impulsive source using two hydrophones H1 and H2 at depths h_i , $i=1,2$. The travel times $t_{d,i}$ and $t_{s,i}$ correspond to the direct (solid) and surface-reflected (dashed) propagation paths.

In this method a ray-theoretic approach [14] for propagation modeling is adopted taking into account acoustic refraction, caused by the spatial variability of temperature, salinity and sound speed with depth. The localization problem is solved using the method of wave-front tracking [15]. This approach is computationally efficient, compared to other localization methods [16,17], and allows for fast, near-real time estimation of the source location, which is a significant advantage for operational localization. The localization (range-depth estimation) method is described below.

The geometry of propagation paths (acoustic rays) is governed by Snell's refraction law [14]

$$\frac{\cos \varphi}{c} = \text{const.} , \quad (1)$$

where φ is the grazing angle of propagation and c the corresponding sound speed. Using eq. (1) the travel time of an acoustic signal propagating along an acoustic ray from depth z_a to depth z_b can be expressed as follows

$$t_{ab} = \int_{z_a}^{z_b} \frac{|dz|}{c(z) \sin(\varphi(z))} = \int_{z_a}^{z_b} \frac{|dz|}{c(z) \sqrt{1 - c^2(z) / \hat{c}^2}} , \quad (2)$$

where $\hat{c} = c_a / \cos \varphi_a$, φ_a is the initial grazing angle and $c_a = c(z_a)$. Eq. (2) applies under the condition that the ray depth is a monotonous function of range. If an acoustic path has turning points or surface reflections, then eq. (2) applies piecewise between turning/reflection points, and the partial times are summed to obtain the total travel time.

Considering a hydrophone at depth h the above relations can be used to a) trace back the geometry of any acoustic ray arriving at the hydrophone with angle of arrival φ , resulting in expressing ray depth as a function of range r and also depending on φ , i.e. $z = z(r; \varphi)$, and b) calculate the time t required for the sound to travel from any point on the ray trajectory to the hydrophone: $t = t(r; \varphi)$. Since t increases monotonically with distance, the inverse of the latter relation can be obtained, such that the range and depth of any arbitrary point on the ray can be expressed as a function of t

$$r = r(t; \varphi, h, c) , \quad z = z(t; \varphi, h, c) \quad (3)$$

depending also on the hydrophone depth h and the sound-speed distribution $c(z)$. Thus, for a particular angle φ and time t , eq. (3) defines a point on the ray arriving at the hydrophone with angle of arrival φ , from which the sound takes time t to reach the hydrophone.

The numerical implementation of eq. (3) for a particular value of the arrival angle φ is performed as follows: The range axis is discretized in equidistant range segments, i.e. in discrete ranges r_j , $j = 1, \dots, J$ from zero (hydrophone position) to a maximum range r_{\max} . Then, using eqs. (1) and (2), the depth z_j and travel time t_j corresponding to each discrete range r_j are calculated (ray tracing) and stored in a lookup table. Since time varies monotonously with range, the discrete travel time t_j can be used as entry to the table, i.e. as an independent variable – this is what eq. (3) represents.

For a particular time t_0 the range and depth in eq. (3) as functions of φ define the locus of points from which the sound takes time t_0 to reach the hydrophone; this locus can also be seen as a wave front that will reach the hydrophone in time t_0 . The geometry of this wave front can be obtained numerically in a simple way by discretizing the angle of arrival. For each discrete value of φ the corresponding lookup table, constructed through ray tracing as described above, is searched for the travel time interval which includes the time t_0 . Taking into account the location of t_0 within this interval the corresponding range and depth are computed by interpolation. Thus, the locus (wave front) for time t_0 is approximated by a series of range/depth points, each one corresponding to a discrete value of φ .

In the following we separate between direct and surface-reflected ray paths: Paths emanating from the hydrophone that do not encounter the surface are direct paths. Paths encountering the surface are considered as either direct or surface-reflected depending on the location of the point of interest on the ray path: for points between the hydrophone and the surface reflection they are considered as direct paths, whereas for points further out they are considered as surface-reflected paths. With this understanding, and using the above relations, the geometry of the direct (d) and surface-reflected (s) rays can be described in the form

$$r_d = r_d(t_d; \varphi_d, h, c) , z_d = z_d(t_d; \varphi_d, h, c) \quad (4)$$

and

$$r_s = r_s(t_s; \varphi_s, h, c) , z_s = z_s(t_s; \varphi_s, h, c) , \quad (5)$$

where the domains of definition for $(t_d; \varphi_d)$ and $(t_s; \varphi_s)$ are different sub-domains of the overall time-angle domain. Expressions (4) and (5), as functions of the arrival angle, describe the two wave fronts arriving at the hydrophone over direct and surface-reflected paths in time t_d and t_s , respectively.

By exploiting the measured differential travel time $t_{sd}^{(m)} = t_s^{(m)} - t_d^{(m)}$ between direct and surface-reflected arrivals, where the superscript (m) denotes measured quantities, and taking the intersection of the direct and surface-reflected fronts given by (4) and (5), for times t_d and $t_s = t_d + t_{sd}^{(m)}$, respectively, we obtain the *isochrone*, i.e. the locus of points having a time difference between the direct and surface-reflected arrivals at the hydrophone equal to $t_{sd}^{(m)}$, see Fig. 2.2,

$$r = r(t_d; h, c) , z = z(t_d; h, c) \quad (6)$$

The above functional relations do not depend on the direct and surface-reflected arrival angles anymore, since for fixed t_d and $t_{sd}^{(m)}$ there are specific values of φ_d and φ_s that satisfy the absolute and differential time constraints.

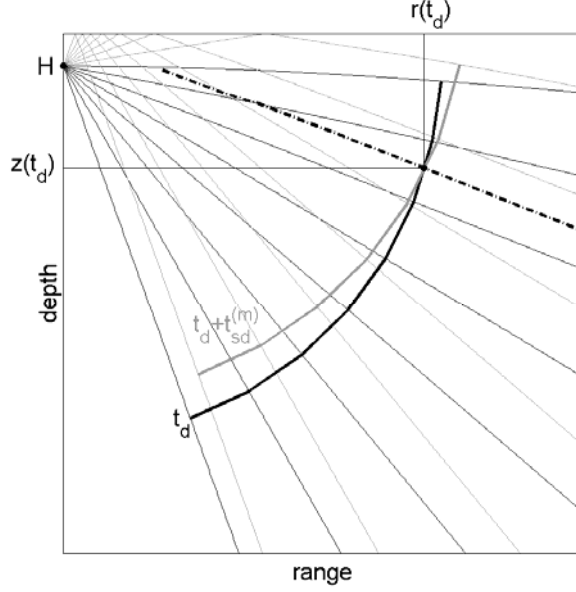


Fig. 2.2 Direct (black) and surface-reflected (grey) ray paths and wave fronts associated with hydrophone H . The dash-dotted line is the isochrone, i.e. the locus of points with travel-time difference at H equal to $t_{sd}^{(m)}$.

In the case of two hydrophones the measured differential travel time between direct and surface-reflected arrivals at each hydrophone can be utilized to establish two isochrones of the form (6), one for each hydrophone ($i = 1, 2$)

$$r_i = r_i(t_{d,i}; h_i, c), \quad z_i = z_i(t_{d,i}; h_i, c), \quad i = 1, 2 \quad (7)$$

where h_i is the hydrophone depth and $t_{d,i}$ is the travel time to each hydrophone along the corresponding direct paths. Considering that both hydrophones pick up the signal from the same source two additional constraints apply: (a) the difference between the direct arrivals at the two hydrophones has to match the corresponding measured differential travel time $t_{21}^{(m)}$

$$t_{21}^{(m)} = t_{d,2} - t_{d,1}, \quad (8)$$

provided that the two hydrophones have a common time reference, and (b) the source depths z_1 and z_2 have to be the same, since they both refer to the same location. The ranges r_1 and r_2 will be different since the two hydrophones will in general be at different locations. Taking into account eq. (8) the localization problem reduces to finding the time $t_{d,1}$ for which the following equation holds

$$z_2(t_{d,1} + t_{21}^{(m)}; h_2, c) = z_1(t_{d,1}; h_1, c), \quad (9)$$

This equation can be solved numerically. In summary, the localization of a source for known hydrophone depths and sound-speed distribution can be performed in the following steps:

- i) Perform ray tracing for the rays emanating at each hydrophone and establish the relations (4) and (5) covering the interval $(-\pi/2, \pi/2)$ for the arrival angle and a time interval spanning the localization domain.
- ii) Using the measured differential travel times between direct and surface-reflected arrivals $t_{sd,1}^{(m)}$ and $t_{sd,2}^{(m)}$, calculate the two isochrones $r_i = r_i(t_{d,i}; h_i, c)$, $z_i = z_i(t_{d,i}; h_i, c)$, $i = 1, 2$, one for each hydrophone.
- iii) Using the measured differential travel time $t_{21}^{(m)}$ between direct arrivals at the two hydrophones, calculate the source depths $z_1(t_{d,1}; h_1, c)$ and $z_2(t_{d,1} + t_{21}^{(m)}; h_2, c)$, as functions of the time $t_{d,1}$.
- iv) Evaluate the time $\hat{t}_{d,1}$ for which the depths z_1 and z_2 coincide; this is the estimated source depth \hat{z} , i.e. $\hat{z} = z_1(\hat{t}_{d,1}; h_1, c) = z_2(\hat{t}_{d,1} + t_{21}^{(m)}; h_2, c)$. The source range with respect to hydrophone i is then $\hat{r}_i = r_i(\hat{t}_{d,i}; h_i, c)$, $i = 1, 2$.

The above localization method relies on the knowledge of the sound-speed profile for the area at the time of interest as well as on the knowledge of the hydrophone depths. The latter need to be monitored continually with an accuracy of $O(0.1 \text{ m})$ rms, otherwise significant localization errors may occur, especially at longer ranges [15]. Further, the accuracy of the localization relies on the precision of the travel time measurements. Errors up to 0.1 msec are acceptable for differential travel times between direct and surface-reflected arrivals. Larger errors, up to 1 msec, can be tolerated in the differential travel time between direct arrivals at the two hydrophones.

3. Experimental data and pre-processing

3.1 The Edelweis'14 controlled localization experiment

The Edelweis'14 experiment took place in the Ionian Sea from 3-11 August 2014 with the R/V Nereis of the Pelagos Cetacean Research Institute. Its objectives were to acquire acoustic data transmitted from a broadband acoustic source (pinger) deployed at a depth compatible with sperm whale diving, in various configurations and setups so as to allow source localization and validation, to acquire concurrent environmental data such as temperature and sound speed profiles to allow sufficient environmental description for propagation model setup, and finally, if possible, to obtain actual sperm whale vocalization acoustic recordings in configurations allowing for animal localization and tracking. The first two objectives (controlled localization experiment and environmental data collection) were accomplished. The last objective was not met due to lack of sperm whale encounters.

3.1.1 Preliminary propagation calculations

For the preparation and planning of the Edelweis'14 experiment a preliminary numerical propagation study was conducted. For that study a historical sound-speed profile from the MODB database [20] was used typical for the Ionian Sea in summer. Figs. 3.1.1.1 and 3.1.1.2 show typical results from that study concerning the transmission loss versus

range and depth for an acoustic source at 100 and 500 m, respectively. The upper two panels in each figure show the ray diagram and the sound-speed profile, whereas the transmission loss is shown in the lower panel.

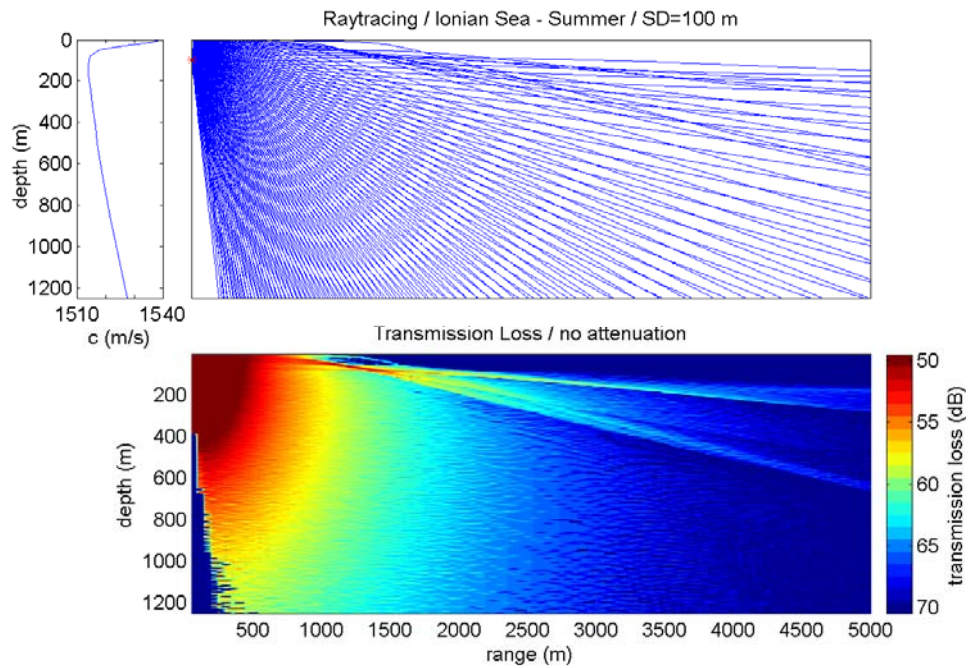


Fig. 3.1.1.1 Propagation calculations using historical sound-speed profile for the Ionian Sea in summer, for a source at a depth of 100 m. The upper panel shows the ray diagram and the sound-speed profile the lower panel shows the transmission loss (no attenuation).

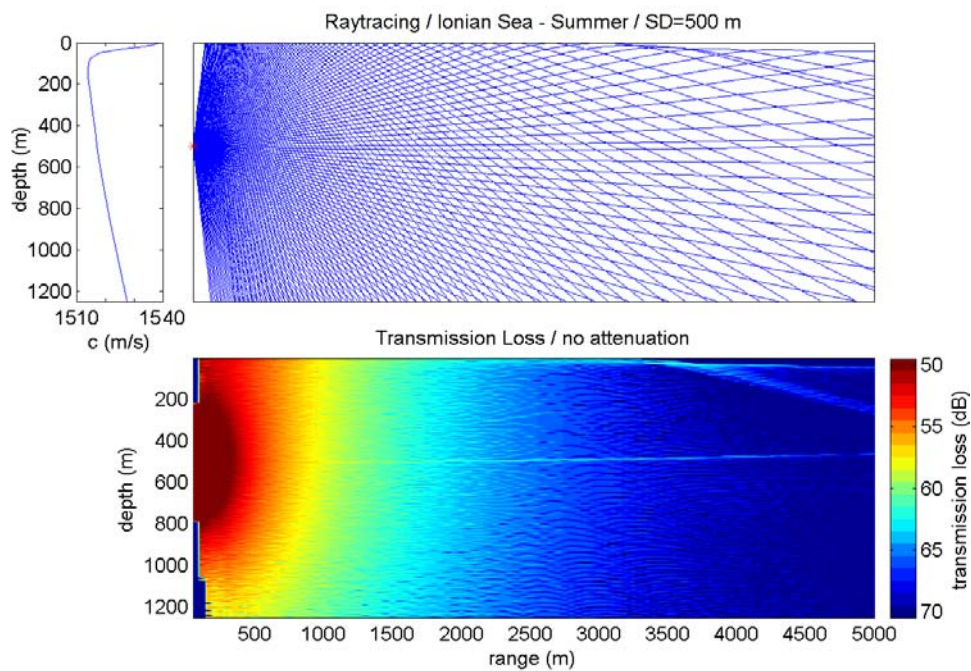


Fig. 3.1.1.2 Propagation calculations using historical sound-speed profile for the Ionian Sea in summer, for a source at a depth of 500 m. The upper panel shows the ray diagram and the sound-speed profile the lower panel shows the transmission loss (no attenuation).

The sound-speed profile is characterized by a minimum at about 100 m (axial depth). The rapid sound-speed increase above that depth causes strong downward refraction. In this connection shallow rays of low grazing angle, such as the ones emanating from the shallow source (Fig. 3.1.1.1) are bent downwards and consequently a shadow zone sets in at shallow depths and relatively small ranges (starting at ~1500 m). This can also be seen in the lower panel in the form of large transmission loss (low acoustic field intensity) represented by the dark blue color. On the other hand when the source is at 500 m depth the rays entering the surface layer are steeper and the effect of refraction is much weaker. Consequently the surface layer is much better ensonified in the case of the deep source. The lesson from these results is that when the acoustic source approaches the surface, e.g. a pinger towed from a moving ship or a sperm whale approaching the surface, the acoustic signals might not be picked up by shallow hydrophones at ranges as small as 2 km, simply because the hydrophones might lie within the shadow zone caused by refraction.

By virtue of the reciprocity principle [14] these results are valid for the case where the locations of source and receiver are switched. In that case Figs. 3.1.1.1 and 3.1.1.2 can be alternatively interpreted as ray diagrams and transmission loss from an arbitrary source location (range and depth in this case are that of the acoustic source) to a hydrophone at depth of 100 and 500 m, respectively.

Figs. 3.1.1.3 and 3.1.1.4 show the predicted time difference between direct and surface-reflected arrivals for an acoustic source at 100 m and 500 m, respectively. The upper panel in each figure shows the dependence of the time difference on the receiver range and depth whereas the lower panel shows the range-depth domain where the time difference is larger than 10 msec. Taking into account the duration (pulse length) of the signals of interest (~5 msec), the latter is a necessary condition – with a sufficient security margin – for the direct and surface-reflected arrivals to be separated (non-overlapping) and distinguishable.

From these figures (lower panels) it is seen that when the source is shallow the hydrophones need to be located at large depth in order to have the direct and surface-reflected arrivals well separated. If the hydrophones are shallow, even if they lie outside the shadow zone (Fig. 3.1.1.1) the received arrivals may be too close or possibly overlap with each other such that they cannot be used for localization. On the other hand, with a deep source, e.g. at 500 m depth, direct and surface-reflected arrivals have a sufficient separation even at shallow depths.

Again, by virtue of the reciprocity principle [14] Figs. 3.1.1.3 and 3.1.1.4 accept an alternative interpretation in which they give the time of arrival difference at a hydrophone at fixed depth (100 m and 500 m, respectively) as a function of source range and depth.

The lesson from the preliminary study was that in the particular environment acoustic receptions at shallow depths are to be expected for large source depths in which case there is sufficient separation between direct and surface-reflected arrivals as well. On the other hand when the source is close to the surface, e.g. pinger during tow or sperm whale ascending to surface,, acoustic receptions at shallow depths should not be expected because the hydrophones may lie in the shadow zone, whereas even in the case that signals are received direct and surface-reflected may be too close to each other or possibly overlap, such that they cannot be used for localization purposes.

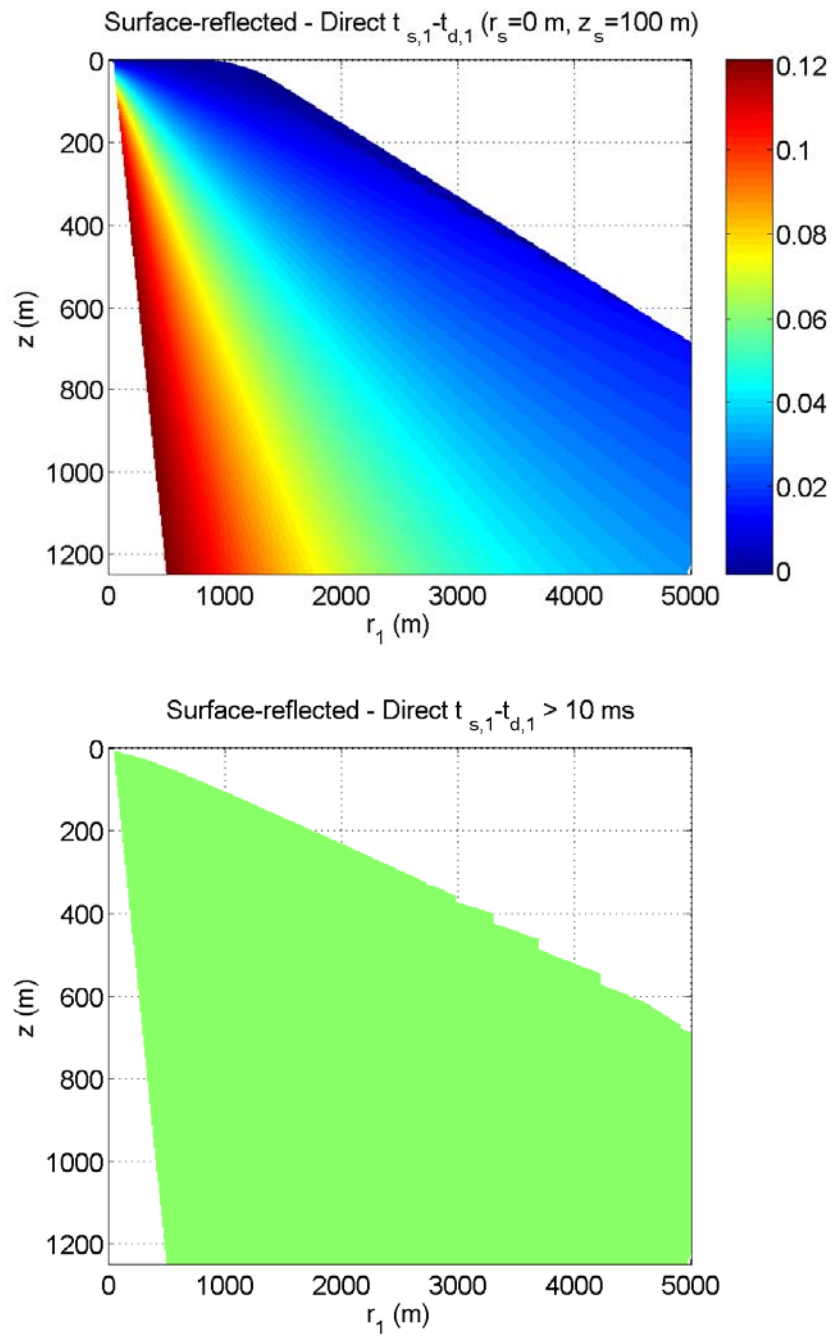


Fig. 3.1.1.3. Top: Predicted time difference between direct and surface-reflected arrivals for an acoustic source at 100 m. Bottom: Range-depth domain where the the time difference is larger than 10 msec.

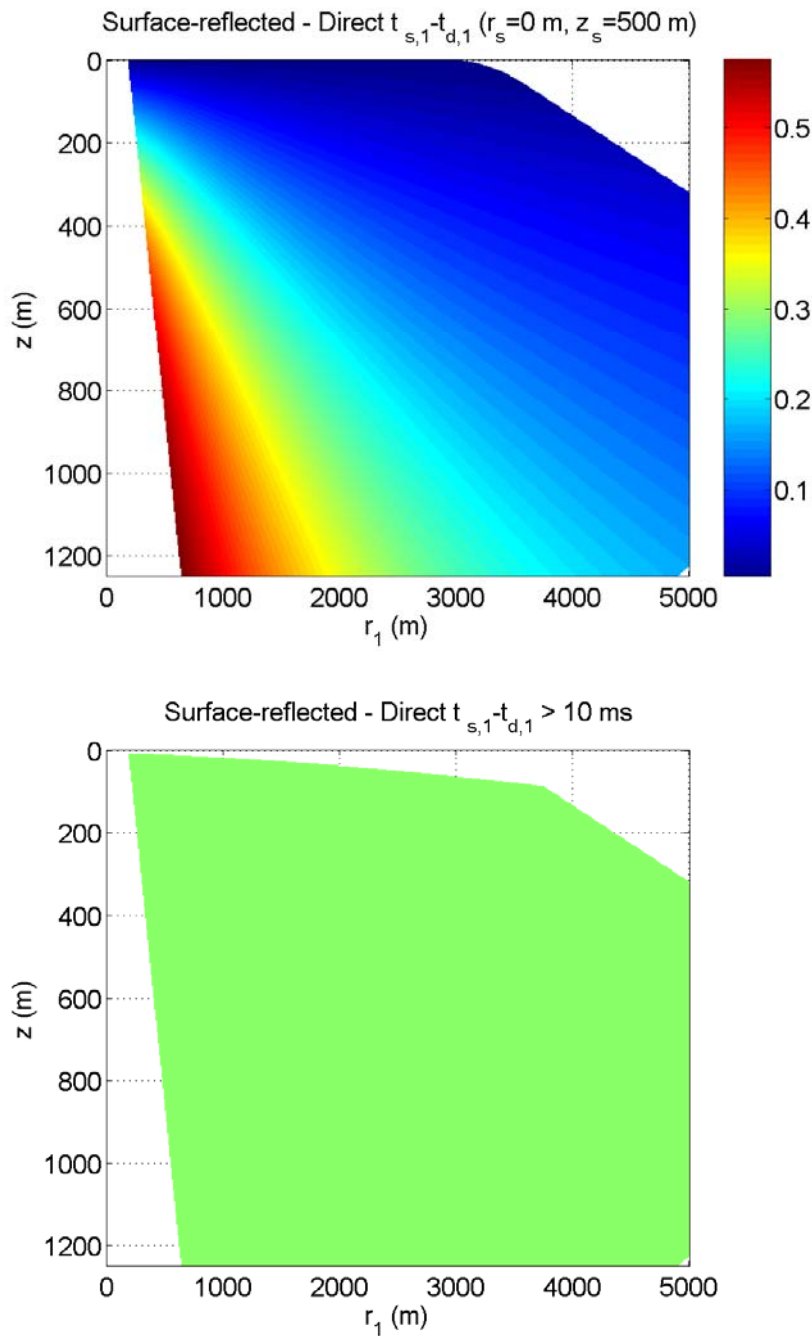


Fig. 3.1.1.4. Top: Predicted time difference between direct and surface-reflected arrivals for an acoustic source at 500 m. Bottom: Range-depth domain where the the time difference is larger than 10 msec.

3.1.2 Experiment implementation

The Edelweis'14 controlled localization experiment which is the objective of the present analysis was conducted on 9 August 2014, between 12 (noon) and 4 pm local time, in a deep-water area (average water depth of 1000 m) SE of the Zakynthos island. The area and the geometry of the experiment is shown in Fig. 3.1.2.1. While the experiment started with good weather, the wind and wave conditions gradually deteriorated and the

experiment had to be shortened. At the start of the experiment two Acoustic Oceanographic Buoys [8], called AOB21 and AOB22, were deployed about 190 m apart. An array of 8 hydrophones was suspended from each buoy. The nominal depths of the lowermost hydrophones of each array were 80 m and 66.3 m for AOB21 and AOB22, respectively. The buoys were free to drift and as a matter of fact they drifted during the experiment at a speed of ~ 0.3 kn in near-south direction [7].

Each buoy recorded the received acoustic pressure at its 8 hydrophones with a sampling frequency of 50 kHz. Further a GPS receiver on each buoy served to provide the buoy location at any time and establish synchronization between the two buoys (GPS time). These data were stored internally in each buoy and partially transmitted in near-real time to the ship via a WLAN link. Unfortunately, due to technical problems the WLAN module of AOB21 was not operational during the experiment. The particular buoy was also characterized by poor performance of the GPS receiver which resulted in loss of location data as well as synchronization problems (see subsection 3.5 below). The hydrophone arrays were also equipped with depth sensors, but these sensors were not operational because of technical limitations.

After the deployment of the two AOBs the ship moved to a distance of ~ 200 m from AOB22 (whose WLAN connection and GPS worked properly such that its distance could be estimated) and the acoustic source was lowered with cable length of 600 m. The actual source depth versus time was measured by an autonomous TDR mounted on the acoustic source. After source deployment the ship moved to larger distances from the AOBs along a line forming an angle of $\sim 45^\circ$ with respect to the line connecting the two AOBs up to a distance of ~ 3 km and kept stations. During these stations there was strong drifting of the ship in southward direction at a speed of ~ 1.2 kn.

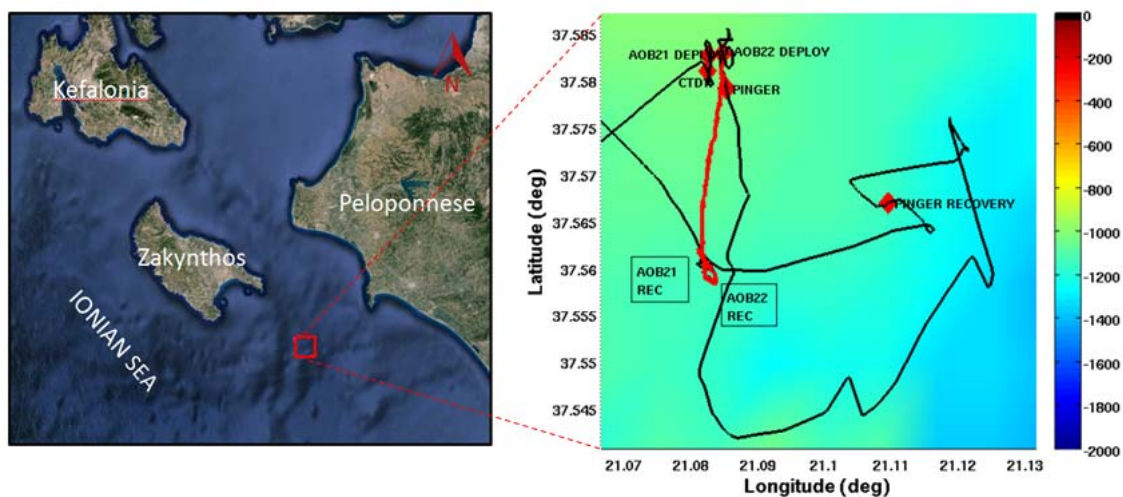


Fig. 3.1.2.1 Area and the geometry of the Edelweis'14 controlled localization experiment

While at the last of these stations (distance of ~ 3 km from AOB22) the source depth was increased by letting another 400 m of cable (total cable length 1000 m). Then the ship moved along a circle centered at the location of AOB22 and kept three more stations – station locations can be identified in Fig. 3.1.2.1 because of the southward drift, see also Fig. 3.2.1.1 below. Then it was realized that the ship was close to endfire location with respect to the two AOBs so it was decided to head towards the buoys and keep two more

stations, one at 2 km and one at 1 km distance. During the first of these stations the weather conditions started rapidly deteriorating. Because of that the last station was skipped, the acoustic source was recovered and then the two AOBs were recovered. In total 8 stations were made. The above mentioned problem with the GPS receiver of AOB21 persisted through all stations except the last one. So the GPS location of AOB21 is available throughout the experiment duration, but that of AOB21 only during the last station.

3.1.3 Shortcomings

AOB21 location data: The GPS receiver mounted on the AOB21 performed poorly (was in contact with less than 3 satellites) over most of the experiment duration. Only during the last station it contacted 4 to 7 satellites. In this connection reliable location data for AOB21 are available only for the last station.

AOB21 communication link: The WLAN module of AOB21 was not operational during the experiment. Because of this the above mentioned GPS malfunction of AOB21 could not be monitored during the experiment, neither its distance from the ship could be estimated. The adjustment of the ship route to the drifting of the buoys was based on the real-time position data from AOB22.

Synchronization: The acoustic signals recorded at AOB21 and AOB22 exhibit unnatural time offsets which points to a synchronization problem between the two AOBs. The malfunction of the GPS system of AOB21, possibly together with other factors, caused this problem.

Hydrophone depths: Due to technical limitations the AOB depth sensors were not operational during the Edelweis'14 experiment. Thus the exact hydrophone depths are unknown.

3.2 Position data

In this section the GPS data for the ship and the two AOBs as well as the depth sensor data for the acoustic source are presented and discussed. By combining the data for the ship route with the source depth data and the known cable length, estimates for the horizontal location of the source and its distance from the AOBs at each station are obtained. Finally, the problem of missing hydrophone depths is discussed and possible intervals of variability are determined.

3.2.1 GPS data (ship and AOBs)

The ship route and those of the two AOBs during the Edelweis'14 controlled localization experiment, based on the GPS data, are shown in Fig. 3.2.1.1. As already mentioned, after the deployment of the two AOBs the ship moved to different locations while towing the acoustic source with cable length 600-1000 m and made 8 stations described in Table 3.2.1.1. These stations are also marked in Fig. 3.2.1.1 where they can also be discriminated by the strong drift which interrupts the line of the ship course.

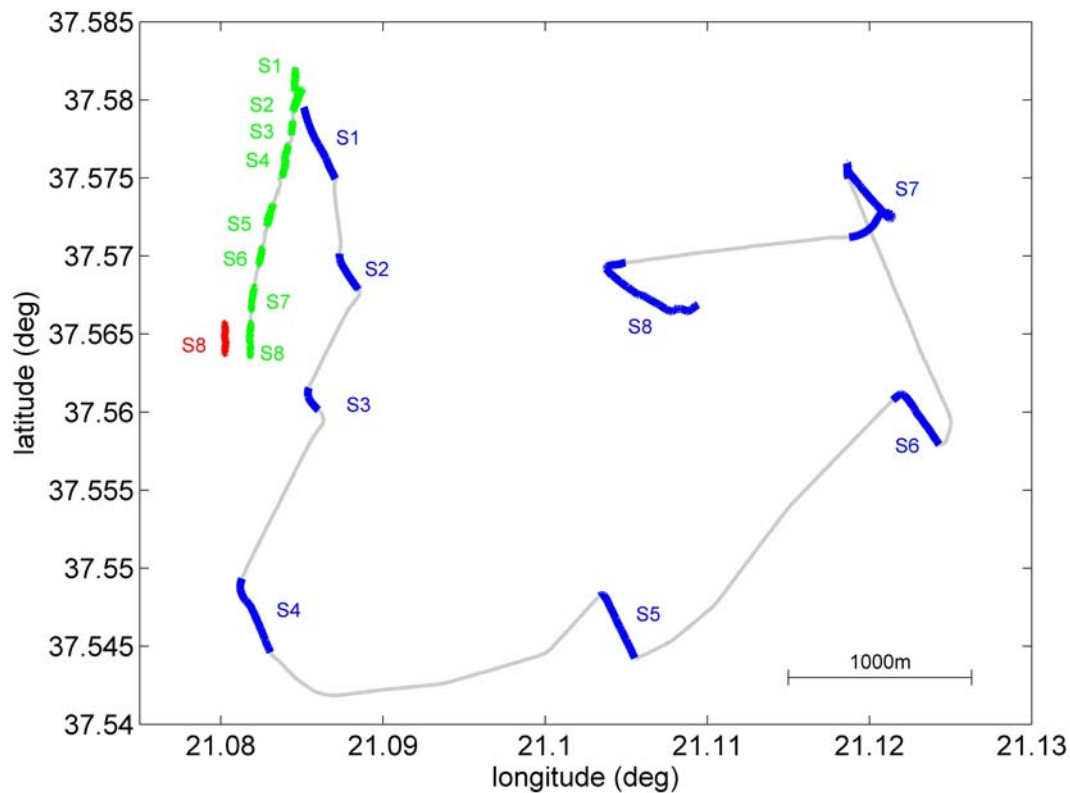


Fig. 3.2.1.1 Ship and AOB routes during the Edelweis'14 controlled localization experiment. The locations of R/V Nereis, AOB21 and AOB22 during the stations are marked in blue, red and green, respectively.

The GPS receiver of AOB22 operated properly throughout the experiment, whereas that of AOB21 exhibited poor performance and only during the very last station managed to get in contact with more than 3 satellites. Fig. 3.2.1.2 shows the number of satellites contacted by the two buoys during the experiment. The light grey areas in this figure indicate the duration of the stations. It is seen that AOB21 contacted a sufficient number of satellites only during the last station. In this connection, reliable location data for AOB22 are available throughout the experiment, nevertheless for AOB21 only during the last station.

3.2.2 TDR data (source depth)

The source depth during the Edelweis'14 controlled localization experiment as measured by the TDR mounted on the acoustic source is shown in Fig. 3.2.2.1. The 8 stations are also marked in this figure by light grey areas. The depth accuracy of the TDR is ± 0.5 m. It is seen that during the tow between stations the source ascends towards the sea surface. When the ship stops the source starts descending. During station S1 the acoustic source was deployed with cable length 600m with the ship on station. As is seen from Fig. 3.2.2.1 it reached a maximum depth of about 500 m after which it started ascending (possibly due to the drifting of the ship). At the end of station S1 the ship reached a distance of ~ 670 m from AOB22 due to southward drift. The ship then moved to station S2 at distance ~ 1000 m from AOB22. During the motion the source rapidly ascended

towards the surface. When the ship stopped the source started descending but reached a depth of only ~180 m. This was possibly due to the strong drift of the ship. The same was repeated in the case of station S3.

Table 3.2.1.1 Station data of Edelweis'14 controlled localization experiment. The two lines for each station correspond to its start and end.

Station name	Local Time	Ship GPS location	AOB21 GPS location	AOB22 GPS location	Ship-AOB22 distance (m)	Source depth (m)
S1	12:30	37° 34' 46.61''N 21° 05' 4.42''E	-	37° 34' 54.93''N 21° 05' 4.42''E	260	10
	12:44	37° 34' 29.58''N 21° 05' 4.42''E	-	37° 34' 50.04''N 21° 05' 4.51''E	665	344
S2	12:49	37° 34' 12.5''N 21° 05' 4.42''E	-	37° 34' 47.47''N 21° 05' 4.62''E	1100	87
	12:55	37° 34' 4.17''N 21° 05' 4.42''E	-	37° 34' 45.43''N 21° 05' 4.16''E	1320	174
S3	13:04	37° 33' 41.91''N 21° 05' 4.42''E	-	37° 34' 42.86''N 21° 05' 3.88''E	1880	35
	13:10	37° 33' 36.5''N 21° 05' 4.42''E	-	37° 34' 40.41''N 21° 05' 3.72''E	1975	166
S4*	13:21	37° 32' 40.62''N 21° 05' 4.42''E	-	37° 34' 37.42''N 21° 05' 2.93''E	3085	23
	13:41	37° 32' 54.93''N 21° 05' 4.42''E	-	37° 34' 30.51''N 21° 05' 1.59''E	3385	519
S5	14:04	37° 32' 53.28''N 21° 05' 4.42''E	-	37° 34' 23.55''N 21° 05' 59.55''E	3295	12
	14:15	37° 32' 39.2''N 21° 05' 4.42''E	-	37° 34' 19.82''N 21° 5' 58.62''E	3685	422
S6	14:35	37° 33' 38.38''N 21° 05' 4.42''E	-	37° 34' 13.75''N 21° 5' 57.21''E	3590	10
	14:45	37° 33' 28.52''N 21° 05' 4.42''E	-	37° 34' 10.22''N 21° 05' 56.36''E	3925	392
S7	15:04	37° 34' 29.67''N 21° 05' 4.42''E	-	37° 34' 4.77''N 21° 05' 55.47''E	3325	12
	15:14	37° 34' 16.38''N 21° 05' 4.42''E	-	37° 33' 59.72''N 21° 05' 54.75''E	3295	702
S8	15:29	37° 34' 10.5''N 21° 05' 4.42''E	37° 33' 56.41''N 21° 05' 48.91''E	37° 33' 56.41''N 21° 5' 48.91''E	2085	79
	15:38	37° 34' 0.78''N 21° 05' 4.42''E	37° 33' 49.55''N 21° 4' 49.06''E	37° 33' 49.05''N 21° 5' 54.53''E	2465	620
* A fishing boat passed close to the buoys at 13:37						

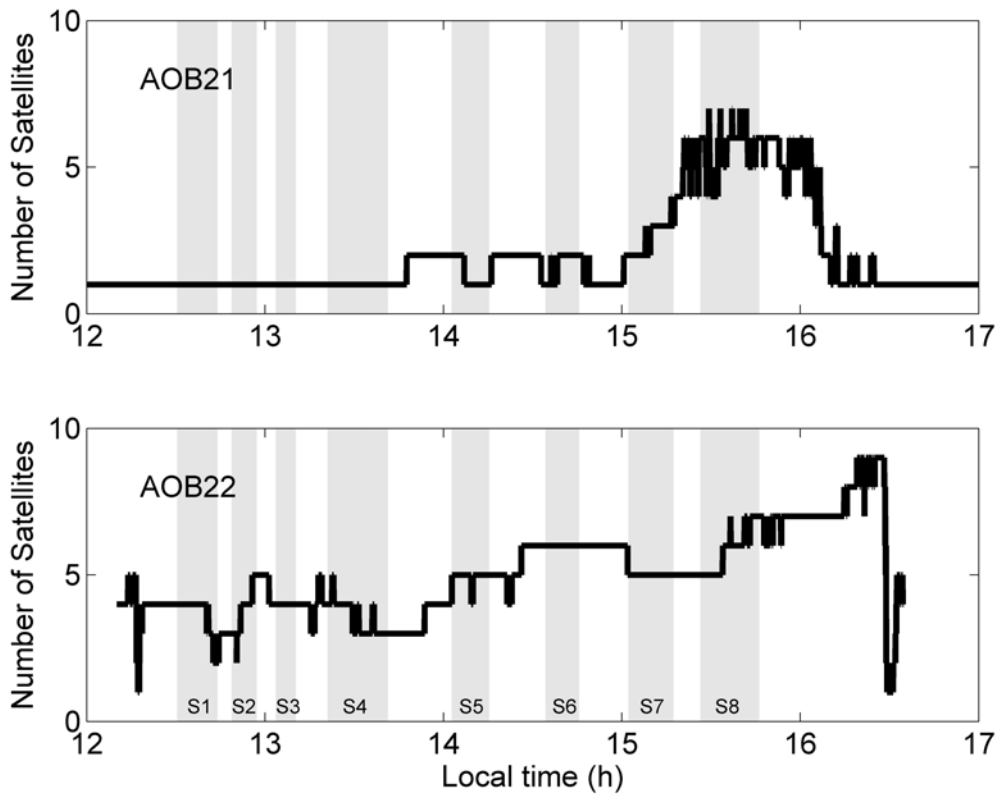


Fig. 3.2.1.2 Number of satellites contacted by AOB21 and AOB22 during the Edelweis'14 controlled localization experiment. The light grey areas mark the 8 stations.

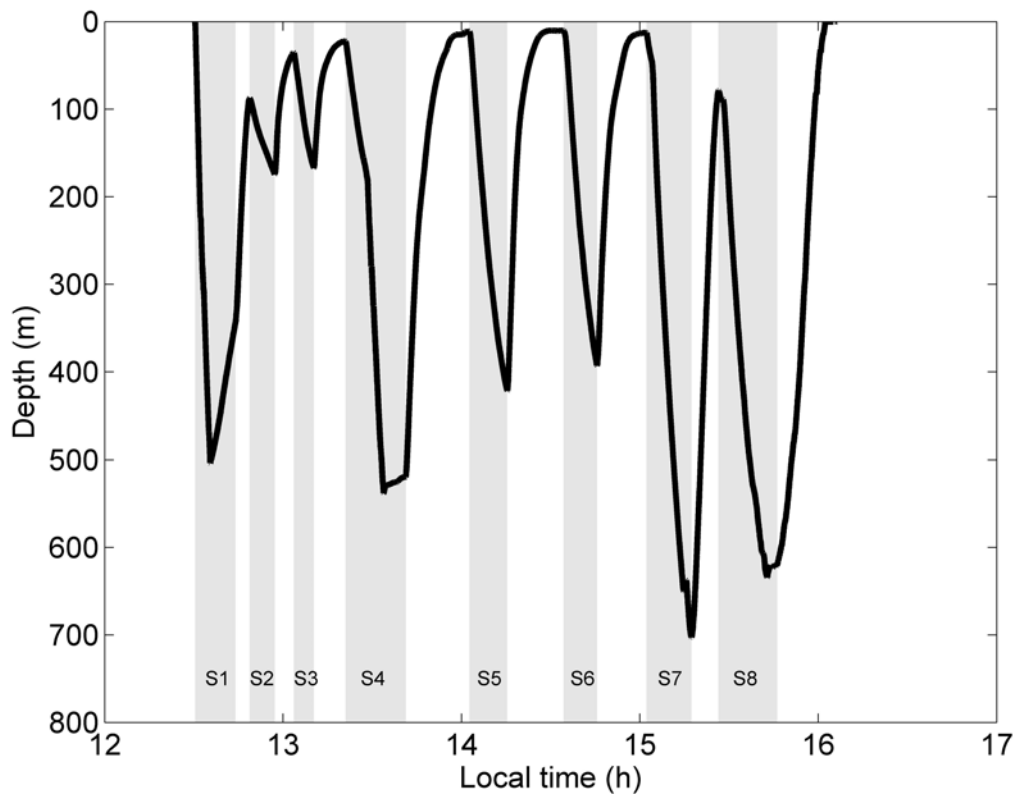


Fig. 3.2.2.1 Source depth during the Edelweis'14 controlled localization experiment. The light grey areas mark the 8 stations.

At station S4 the source initially reached again about the same depth (~200 m) but then additional 400 m of cable was released and the source reached a maximum depth of ~550 m. Right after that the source started slowly ascending, possibly due to the ship drift. The moment of the cable release can be distinguished in Fig. 3.2.2.1 from the knee in the descent. After station S4 the ship attempted to move on a circle centered at the AOBs and perform stations (S5, S6 and S7) on the periphery. During the stations S5 and S6 the ship drift had a backward component compared to the ship course and this in combination with the longer cable length (1000 m) contributed to the somewhat larger descent of the source to ~400 m. This was even more intense in the case of station S7 where the drift was practically opposite to the ship course causing the ship to move backwards while at station. The backward movement probably relaxed the tension at the tow cable and allowed the source to sink as deep as ~700 m, the largest depth reached during the experiment. While at station S7 it was estimated that the ship should be close to the endfire direction with respect to the two AOBs (this could not be easily seen at the time since there was no communication with AOB21), so it was decided to head towards AOB22 to close the loop. On the way one last station (S8) was kept. During that last station the source reached a maximum depth of ~630 M.

3.2.3 Estimated source-receiver ranges

By combining the information about the course of the ship prior to a station with the ship position data while at station (drift direction and intensity), as well as with the data for the source depth (from the depth sensor) and the information about the cable length released in the water, approximate estimates for the horizontal location of the source can be obtained. Combining the resulting areas with the actual location of the AOBs, the ranges (horizontal distances) between the source and the buoys can be estimated to serve as verification data for checking localization performance. During stations S3, S5 and S6 no acoustic TOAD data are available (due to unfavourable combinations of source range and depth – see Section 3.1.1). In the following the assumptions for the source locations at the 5 remaining stations are presented.

Station S1. During this station the acoustic source is lowered with cable length 600 m. During the deployment the ship is drifting southwards. In this case the source is assumed to lie between the initial deployment position (position of the ship at the start of source deployment) and the actual ship location.

Stations S2 and S4. During the tow towards the station the source ascends towards the surface, i.e. lies behind the ship at a distance about equal to the cable length. So at the start of station the source lies a cable length behind the ship location at station start. During the station the closest possible location of the source to the AOBs is estimated assuming the cable to form a straight line and taking into account the source depth (from the depth sensor) – the larger the source depth the closer the horizontal location of the source to the ship location. The farthest possible location of the source from the AOBs is separated from the actual ship location by the cable length reduced by the actual source depth. This corresponds to the limit where the cable remains near-horizontal close to the ship (as during the tow) and near-vertical on the side of the source (gamma shape).

Station S7. Taking into account that the course of the ship prior to station S7 is nearly tangential to the circle centred at the AOB locations and that the drift is practically opposite to the ship course causing the ship to move backwards while at station the location of the poinger is assumed to lie on the line of the ship course with allowed

deviation $\pm 10^\circ$ from the ship longitudinal axis. With cable length of 1000 m this results in a corridor for the possible source location of ± 173 m about the ship route.

Station S8. During station S8 the drift has a strong backward component such that the tow cable tension is probably relaxed during the first phase of the station. This allows the acoustic source to sink fast, as shown in Fig. 3.2.2.1. During the station the ship moves side- and backwards and this probably leads the cable to resume tension at a certain point, causing the source to move towards the ship. The farthest possible location of the source from the AOBs is taken as the initial location of the source at the station start. To estimate the limit for the closest possible location of the source to the AOBs, the location in the middle between the ship and the source at the station start is taken.

The resulting range limits referring to AOB21 and AOB22 during the above stations are shown in Fig. 3.2.3.1. It is seen that the range uncertainties for the stations S4, S7 and S8 are between 400 and 500 m. They are smaller for the first station (S1) whereas during the move to S2 the variability interval narrows further down because of the approach between the lower and the upper limit. These range intervals will be used in the localization, section 4, for verification purposes.

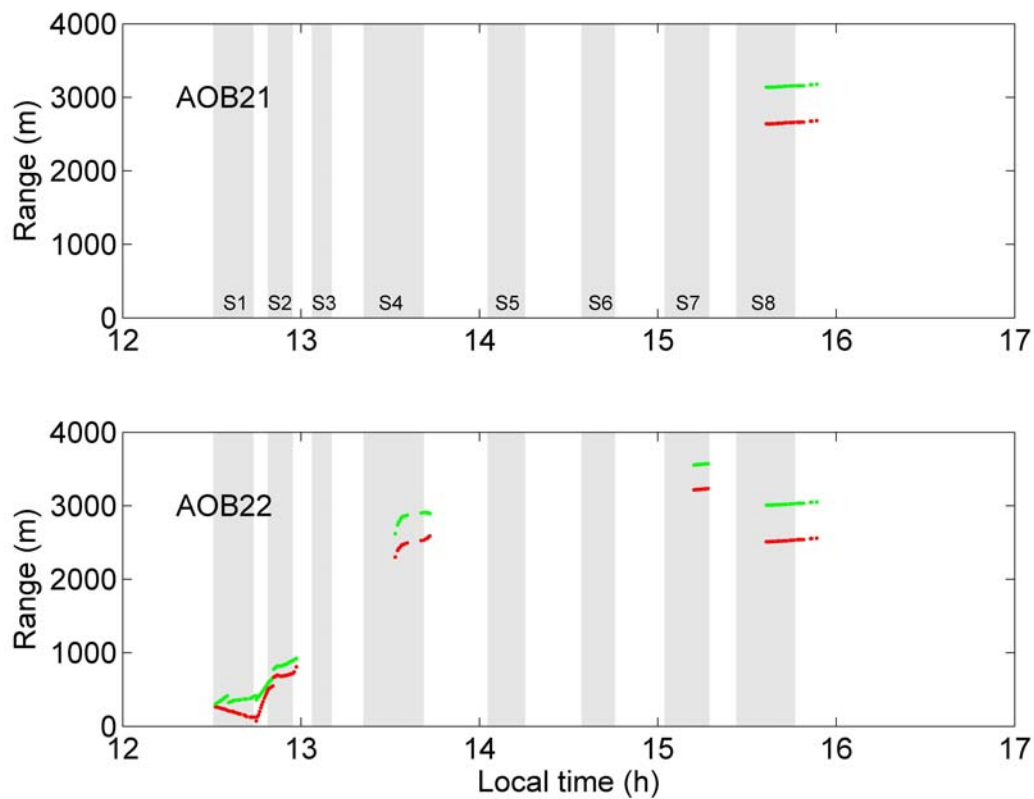


Fig. 3.2.3.1 Estimates for lower (red) and upper (green) range limits between the source and AOB21 (top), the source and AOB22 (bottom) during stations S1 S2 S4 S7 and S8. The light grey areas mark the 8 stations.

3.2.4 Hydrophone depths

As already mentioned, due to technical limitations the AOB depth sensors were not operational during the Edelweis'14 experiment. Thus, the actual hydrophone depths are unknown. This is a serious problem since the localization method relies on the precise knowledge of hydrophone depths. The possibility of using the nominal hydrophone depths for the inversions cannot be justified since the two arrays were probably tilted due to the drifting of the AOBs. On the other hand these nominal values can be used to set limits for the intervals of variability of the hydrophone depths.

For AOB21 (nominal depth for lowermost hydrophone 80 m) a variability interval between 75 and 81 m is considered. For AOB22 (nominal depth for lowermost hydrophone 66.3 m) a variability interval between 63 and 67 m is considered.

3.3 Travel-time data

In this subsection the acoustic travel-time data at the lowermost hydrophones of the two AOBs are presented. The emitted signal, shown in Fig. 3.3.1, is a sinusoid with central frequency 11.15 kHz, duration 5 ms (box-shaped envelope) and repeat period 5 sec.

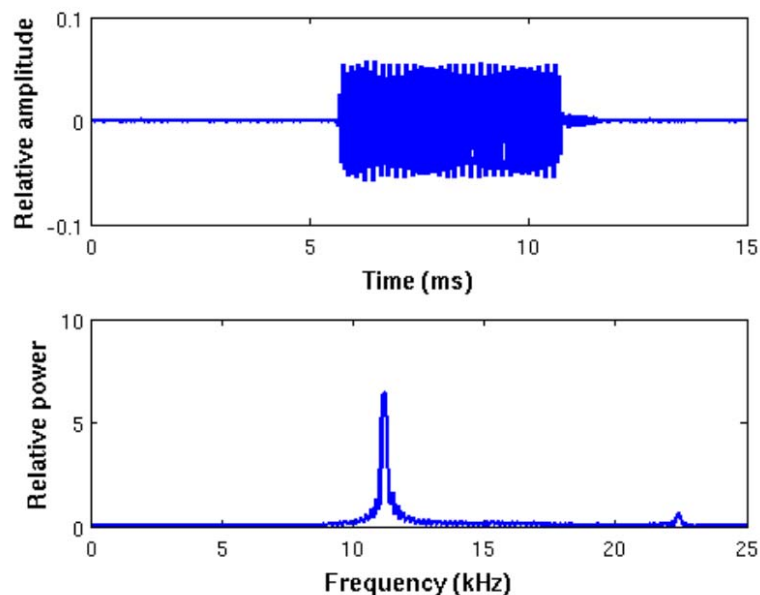


Fig. 3.3.1 The emitted signal in the time (top) and frequency (bottom) domain

3.3.1 Raw data

The acoustic receptions at each hydrophone are stored in 24-sec records with sampling frequency 50 kHz. Fig. 3.3.1.1 shows two typical 24-sec receptions at the lowermost hydrophone of AOB22 during stations S1 (left – the acoustic source lies at 600 m depth and at a horizontal distance of about 300 m) and S7 (right – the source lies at 730 m depth and at a horizontal distance of about 3500 m). Four signals are included in total in each record. The recorded time series (raw signals) are shown at the top of the figure. It is very difficult to see the source signal in the raw receptions, especially at the longer range (right) due to low-frequency noise (wave modulation etc.). The lower panels show the corresponding spectrograms where the different frequency components can be

isolated. The source signal can be seen in the frequency band around the central frequency of 11.15 kHz in the short-range reception. In the long-range spectrogram (right) the signal still cannot be seen because of its low level.

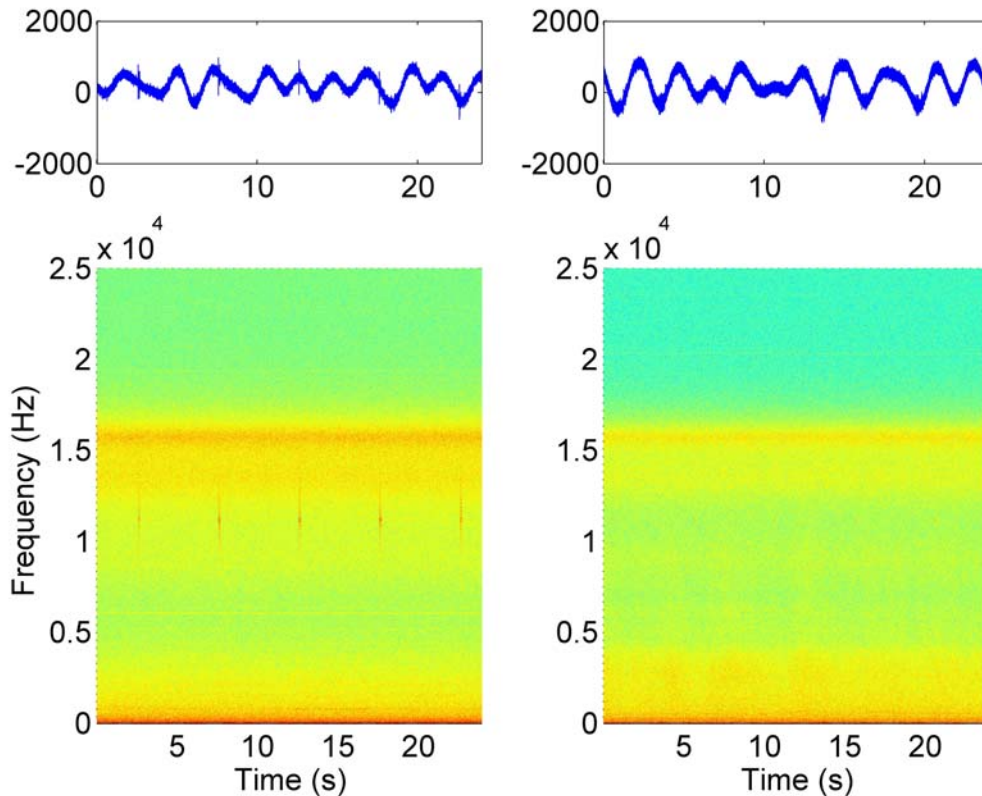


Fig. 3.3.1.1 Typical 24-sec receptions at the lowermost hydrophone of AOB22 during stations S1 (left) and S7 (right) picked up by the lowermost hydrophone of AOB22. The upper panels show the recorded time series (raw signals). The lower panels show the corresponding spectrograms.

3.3.2 Pre-processing (filtering + energy filter)

The upper panels of Fig. 3.3.2.1 shows a filtered version of the recorded time series of Fig. 3.3.1.1. A band-pass filter between 10.1 kHz and 12.1 kHz is used for this purpose. After suppression of the noise (especially of the low-frequency noise) the four signals can now be seen in both cases. The lower panel shows the output of the energy filter applied to the receptions above. The energy filter [10] is a moving average of the squared reception over a window length equal to the pulse duration, i.e. 5 msec. This leads to a further increase of the signal-to noise ratio which is particularly useful in the case of the longer-range reception on the right. Both in the short- and long-range time series each reception is double peaked.

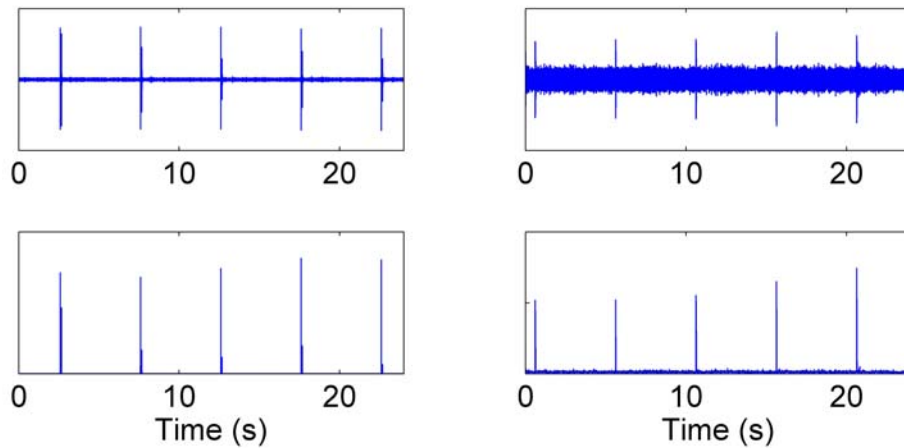


Fig. 3.3.2.1 Typical 24-sec receptions at the lowermost hydrophone of AOB22 during stations S1 (left) and S7 (right) picked up by the lowermost hydrophone of AOB22. The upper panels show frequency filtered receptions. The lower panels show frequency and energy filtered receptions.

This is seen more clearly in Fig. 3.3.2.2 which shows a detailed view of the first reception of the above two records, frequency filtered at the top, frequency and energy filtered at the bottom. The first of the double arrivals in each reception corresponds to the direct acoustic path connecting source and receiver. The second arrival corresponds to the surface-reflected path. The 5 msec pulse arriving via the two paths can be seen in the upper panels of Fig. 3.3.2.2. In the lower panels the energy filter output is shown. The latter provides a robust vehicle for the estimation of time of arrival differences and is used in the following.

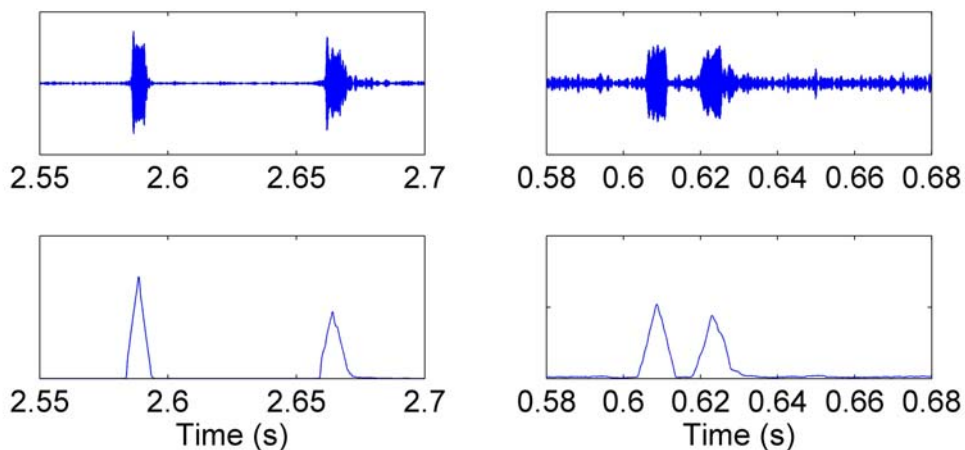


Fig. 3.3.2.2 Detail of receptions shown in Fig. 3.3.2.1 during stations S1 (left) and S7 (right) picked up by the lowermost hydrophone of AOB22. The upper panels show frequency filtered receptions. The lower panels show frequency and energy filtered receptions.

3.3.3 Differential travel times between direct and surface-reflected arrivals

Fig. 3.3.3.1 shows the time of arrival differences (TOADs) between direct and surface-reflected arrivals at the lowermost hydrophone of AOB21 during the Edelweis'14 controlled localization experiment. Similarly, Fig. 3.3.3.2 shows the time of arrival differences between direct and surface-reflected arrivals at the lowermost hydrophone of AOB22. The periods of the 8 stations are also marked on these figures by light grey areas. During the first station (S1 – source deployment) the source descent is seen in Figs. 3.3.3.1 and 3.3.3.2 through the increase or the TOAD between direct and surface reflected arrival, in agreement with the predictions in subsection 3.1.1 – at a given range, the deeper the source the larger the difference in length between the direct and the surface-reflected path from the source to the hydrophone and thus the larger the corresponding TOAD. The ascend of the hydrophone at the end of station S1 is then seen as a decrease of TOADs. During station S2 the hydrophone descends (to smaller depths though) and the TOADs increase again.

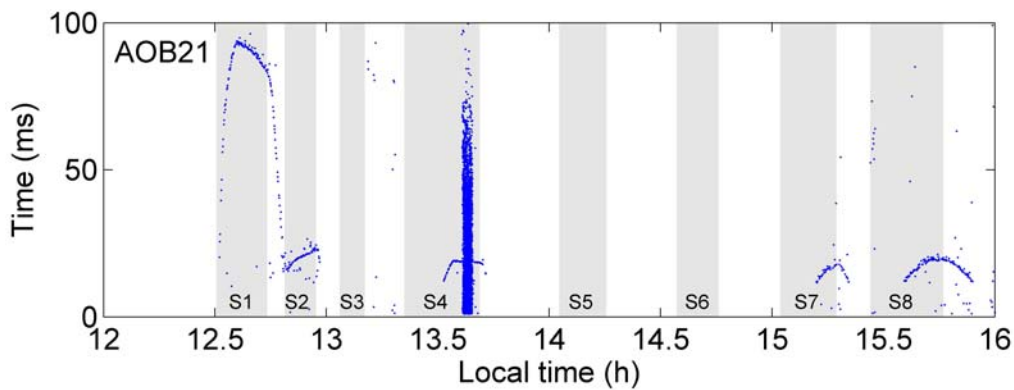


Fig. 3.3.3.1 Time of arrival differences between direct and surface-reflected arrivals at the lowermost hydrophone of AOB21. The light grey areas mark the 8 stations.

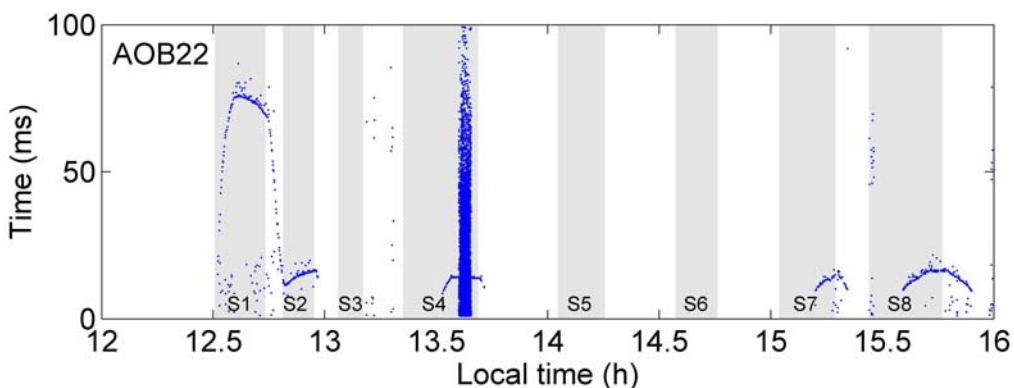


Fig. 3.3.3.2 Time of arrival differences between direct and surface-reflected arrivals at the lowermost hydrophone of AOB22. The light grey areas mark the 8 stations.

After station S2 the source ascends due to the tow and its distance from the AOBs increases such that it enters the shadow/no-resolution zones and TOAD data is no longer

available (the depth of the shadow/no-resolution zones increases with range, cf. Figs 3.1.1.1, 3.1.1.3). During station S3 no acoustic TOADs are observed. The reason is the small depth (less than 180 m) that the source reaches during that station which in combination with the longer range (~2 km) puts the source in the above shadow/no-resolution zones. The same would have occurred in the case of station S4, had no additional cable been released. With the 400 m additional cable the hydrophone reached a depth of ~550 and could be received by the hydrophones at ~3.2 km distance. However, during the station (S4) a fishing boat passed close to the buoys (cf. table 3.2.1.1) which lead to large increase of noise level in the recordings. This is seen in Figs. 3.3.3.1 and 3.3.3.2 in the middle of station S4.

During stations S5 and S6 there are no TOAD data. This is again due to the combination of long-range (~3.5 km – longer than that of station S4) and shallow depth (about 400 m) belonging to the shadow zones and/no-resolution zones of the two hydrophones.

During station S7 the acoustic source performs a deep dive and is sufficiently received by the two hydrophones despite the long range (~3.5 km). The corresponding TOADs between direct and surface-reflected arrivals point to the descend (TOAD increase) and the ascend (TOAD decrease) of the source before and after the moment where it reached maximum depth (~730 m). Finally a similar situation is observed in the case of the last station S8 during which the source reached a smaller depth (~630 m) while at a smaller range (~2 km).

3.3.4 Differential travel times between direct arrivals at AOB21 and AOB22

The estimation of time of arrival differences between direct arrivals at the lowermost hydrophones of AOB21 and AOB22 requires synchronization of the two buoys. Unfortunately during the Edelweis'14 experiment there was a synchronization problem between the two AOBs which prevents the direct use of the measured TOADs. On the other hand, it was fortunate that the correction of this problem turned out to be a matter of addition of a single offset – addition of 2.97354 sec to AOB21 data. The estimation of the time offset (offset calibration) between AOB21 and AOB22 is addressed in subsection 3.5 below.

Fig. 3.3.4.1 shows the offset-calibrated TOADs between direct arrivals at the lowermost hydrophones of AOB21 and AOB22 (time of arrival at AOB22 minus time of arrival at AOB21 – positive means that the signal arrives at AOB21 first, i.e. source closer to AOB21). Data are shown only for the cases where full TOAD sets (three TOADs) are available: TOADs between direct and surface-reflected arrivals at both AOBs and TOADs between direct arrivals at the two AOBs. This is the case only during stations S1, S2, S4, S7 and S8. Data from the stations S3, S5 and S6 are absent due to unfavourable source range and depth combinations belonging to shadow/no-resolution zones. The evolution of TOADs between direct arrivals is related with the azimuthal position (bearing) of the source with respect to the line connecting the two AOBs and in this connection it exhibits a smooth evolution.

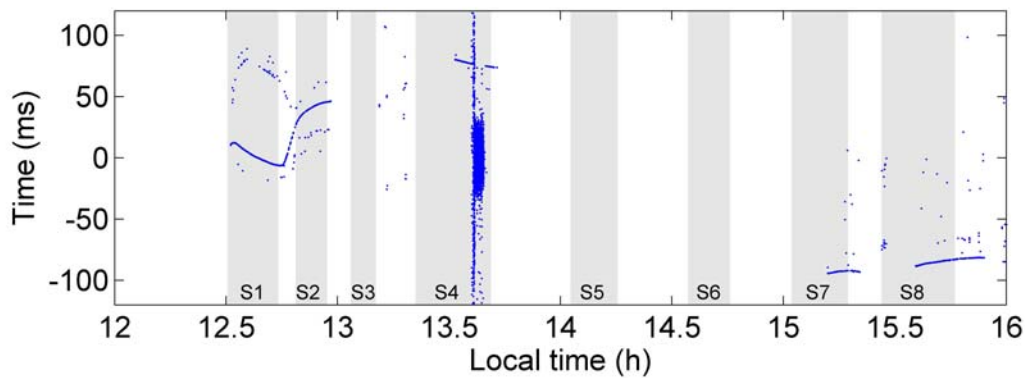


Fig. 3.3.4.1 Time of arrival differences between direct arrivals at the lowermost hydrophone of AOB21 and AOB22 (positive means that signal arrives at AOB21 first) . The light grey areas mark the 8 stations.

3.4 Measured sound-speed profile

The temperature and sound-speed profile obtained from the TDR mounted on the towed source is shown in Fig. 3.4.1. The Chen-Millero formula [11] is used for the calculation of the sound speed from temperature assuming a salinity value of 39 ppt (max. value obtained from the near-surface CTD casts). The temperature rapidly decreases with increasing depth, from $\sim 25^{\circ}\text{C}$ at the surface to less than 15°C at 500 m depth. This temperature decrease in combination with pressure increase results in a sound-speed profile with a shallow channel axis (depth of sound-speed minimum) at ~ 130 m. Strong downward refraction is anticipated for acoustic rays travelling in shallower water layers with strongest effects at depths between 10 and 20 m where the sound-speed slope (with respect to depth) is largest. For the lowermost hydrophones at depths of 80 m (AOB21) and 66 m (AOB22) this means that both direct and surface reflected rays to the hydrophones and the corresponding travel times are affected by refraction, but mostly the surface-reflected ones traversing the 10-20 m depth layer.

3.5 Model-based synchronization – offset calibration

The lack of synchronization data between the two AOBs poses a major problem for the localization, since the TOAD between direct arrivals at the two hydrophone, which is one of the three TOADs used in the localization analysis, relies on synchronization. A possibility to cope with this problem is to use position data (GPS data) for the two AOBs and the ship (acoustic source) in combination with environmental data and propagation modeling in order to predict the TOAD between direct arrivals at the two hydrophones, compare the predictions with the observed TOADs and correct (offset) the latter accordingly.

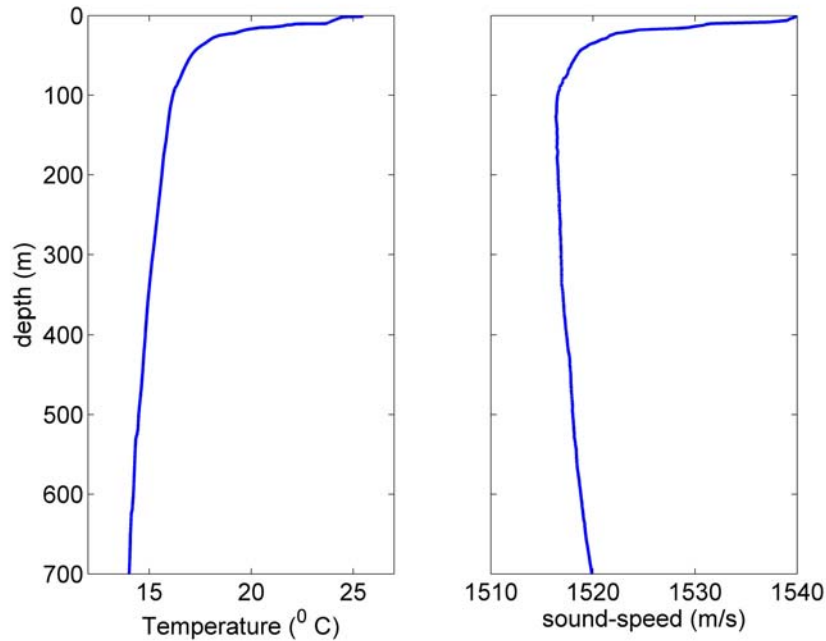


Fig. 3.4.1 Temperature (left) and sound-speed (right) profile in the area of the experiment obtained from the TDR mounted on the source.

A problem in this approach is the lack of GPS data for AOB21 for most of the experiment. Only during the last station S8 the GPS of AOB21 worked properly so the offset calibration can only be based on data from that station. Another question has to do with the location of the acoustic source, since the GPS data refer to the ship location and not to the source which is towed/suspended from the ship with 1000 m cable during S8. In this connection the maximum ranges estimated in subsection 3.2.3 will be used – since the source at station S8 lies at a large distance (~ 3 km) and close to the endfire position of the AOBs the exact range does not play a major role for the direct arrival TOAD at the two hydrophones.

A further problem has to do with the peak identification, i.e. the association between peaks in the recordings of the two buoys. Fig. 3.5.1 shows two corresponding 24-sec records, one from the lowermost hydrophone of each AOB, from the first station S1. The receptions in each record are separated by 5 sec, the pinger repeat period. From this figure it is seen that the receptions at the two AOBs are 2-3 sec apart! This simply cannot be, since the distance between the two buoys is only ~ 130 m which corresponds to less than 0.1 sec TOAD for an acoustic signal travelling at ~ 1500 m/sec. Besides the offset problem this points to an serious association problem. Had the offset been of the order of 0.1 sec, then the association would be clear. Now it is unclear whether each reception at AOB21 corresponds to the previous or the next or perhaps some other reception at AOB22.

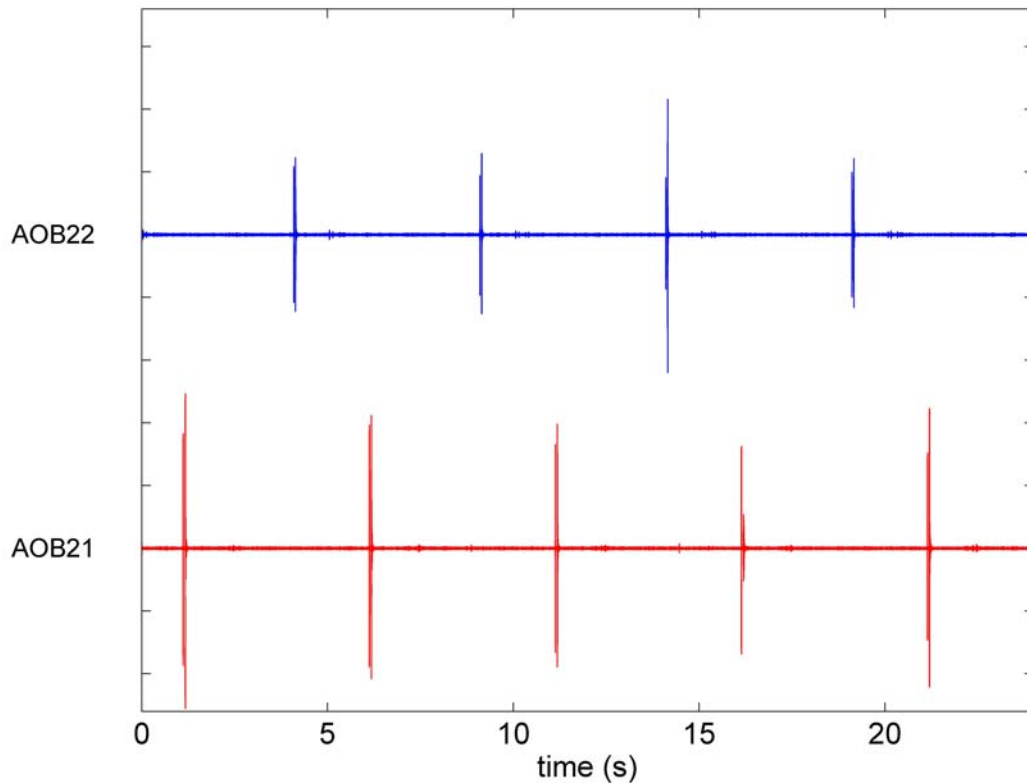


Fig. 3.5.1 Two corresponding 24-sec records from AOB22 (top) and AOB21 (bottom) during station S1.

This problem can be solved by looking at the very first signals emitted by the pinger when it first entered the water. This is a characteristic sequence of signals with non-uniform spacing which can be easily identified. Fig. 3.5.2 shows the corresponding 24-sec records from the lowermost hydrophones of the two AOBs at the beginning of station S1, when the pinger was put in the water. The offset between the two buoys is similar as in Fig. 3.5.1. The ambiguity of peak association is solved by looking at this figure: The arrivals at AOB22 are delayed by ~ 3 sec. Based on that, each reception at AOB21 in Fig. 3.5.1 is associated with the *next* reception on AOB22, *not* with the previous one. This rule is followed in the subsequent analysis.

After solving the association problem the offset calibration problem is addressed by using data from station S8. In particular a reception (control reception) is used which corresponds to one of the deepest source locations, at a depth of 624.1 m. This is the second reception in the 24-sec file named AOB2-221124309.vla corresponding to AOB21 and the second reception in the 24-sec file named AOB2-221124308.vla corresponding to AOB22. At the time of the particular reception the estimated maximum range between the acoustic source and AOB21 is 3153 m. The corresponding range between the source and AOB22 is 3021 m. Using a ray-tracing code and the measured sound-speed profile (Fig. 3.4.1) the eigenrays connecting the source and each of the lowermost hydrophones of each AOB and the corresponding travel-times are calculated. For that calculations the hydrophones are assumed at depths of 80 m for AOB21 and 66 m for AOB22. The calculated direct and surface-reflected eigenrays are shown in Fig. 3.5.3.

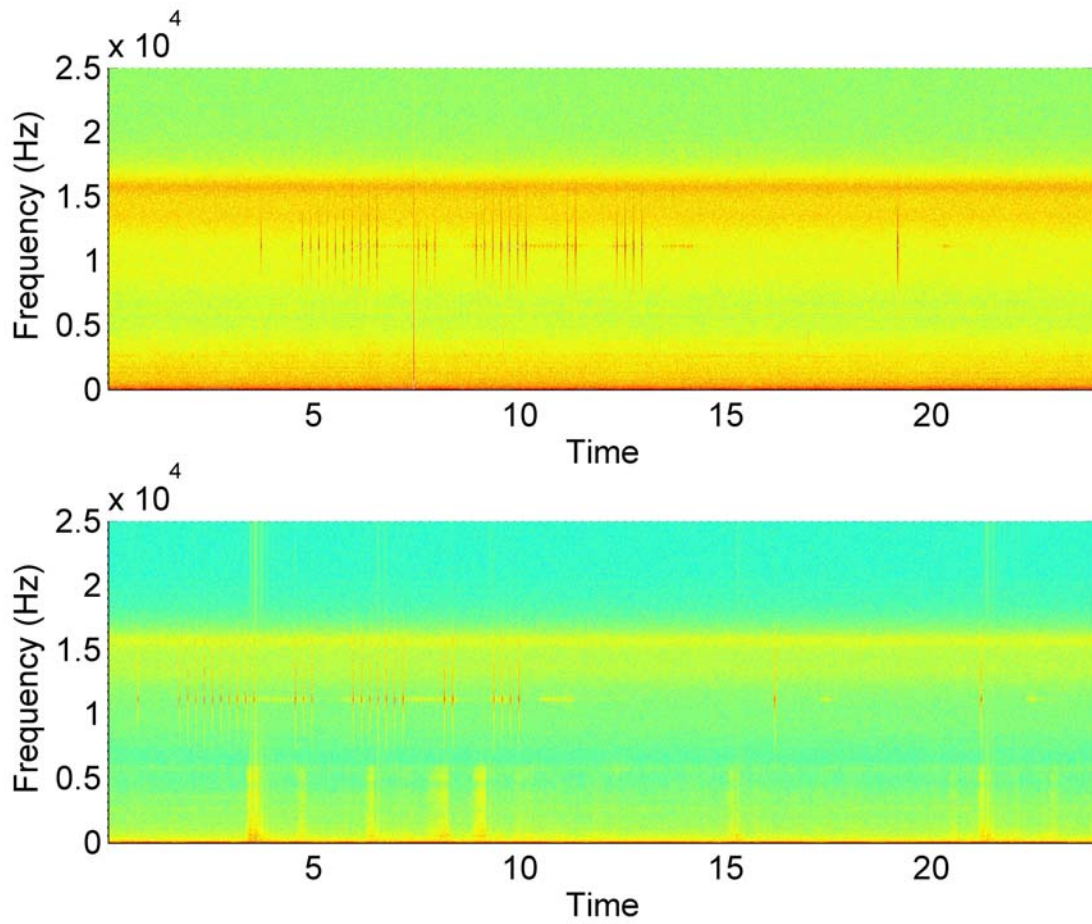


Fig. 3.5.2 Corresponding 24-sec records from AOB22 (top) and AOB21 (bottom) at the beginning of station S1 including control pings for acoustic source.

Fig. 3.5.4 shows the control reception (energy-filter output) recorded at the two AOBs, as obtained from the corresponding 24-sec records, along with the ray-theoretic predictions of the direct and surface-reflected arrivals at each AOB. In this figure the ray-theoretic prediction is aligned with the control reception at AOB22, whereas the original offset between the AOB21 and AOB22 records is retained. It is clear that this offset (close to ~ 3 sec) is unrealistically large.

In Fig. 3.5.5 the reception at AOB21 is shown shifted to the right by 2.97354 sec such that it meets the ray-theoretic prediction. This figure focuses on the time of the receptions in order to show details. It is now clear that the receptions are in agreement with the ray-theoretic predictions, not only the TOAD between the direct arrivals at the two buoys (offset calibration) but also the TOADs between direct and surface-reflected arrival at each buoy – the small deviations are possibly due to deviations of the actual hydrophone depths from the values used in the ray-theoretic predictions (80 and 66 m, respectively). Fig. 3.5.6 shows the 24-sec records from the lowermost hydrophones of the two AOBs during station S1, cf. Fig. 3.5.1, with a time-offset correction of 2.97354 sec applied to AOB21 data. It is seen that the corresponding signals are now much better aligned than in Fig. 3.5.1 (of course there are fine-scale changes due to the different propagation paths that cannot be seen in this figure). Thus, the offset of **2.97354 sec**, estimated from the

data of the last station (S8) will be used as a general offset correction in the following. This correction has already been used in Fig. 3.3.4.1 presented in subsection 3.3.4 above.

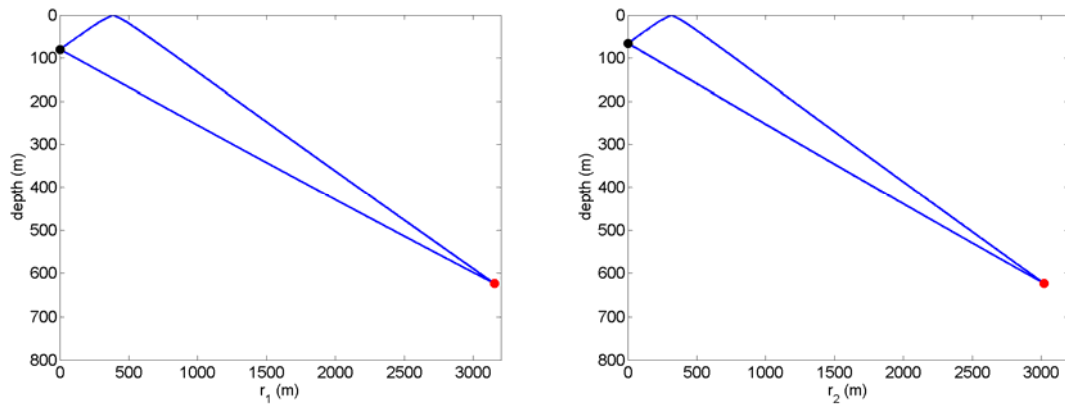


Fig. 3.5.3 Direct and surface-reflected eigenrays connecting the source and the lowermost hydrophone of AOB21 (left) and AOB22 (right), assuming the sound-speed profile of Fig. 3.4.1, source depth 624.1 m, source range from AOB21 3153 m, and source range from AOB22 3021 m.

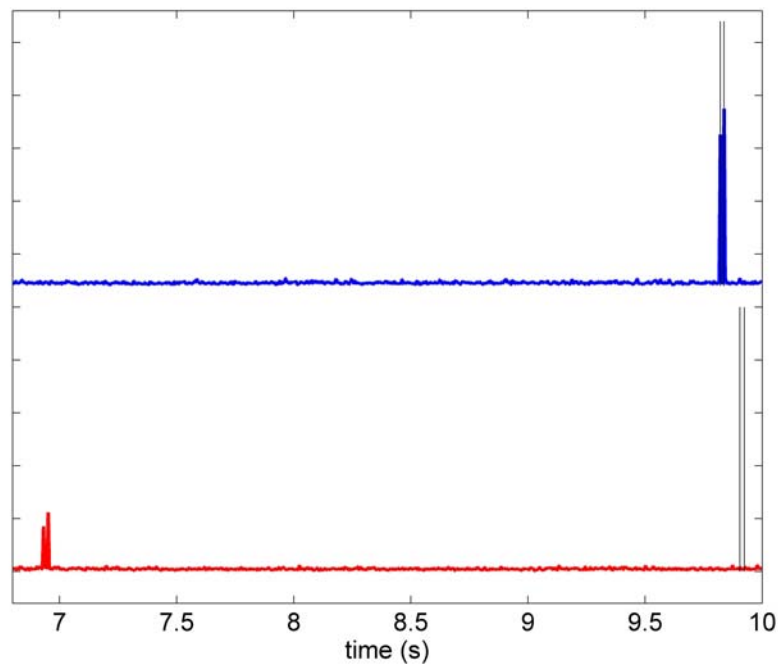


Fig. 3.5.4 Calibration reception (energy-filter output) recorded at AOB22 (top) and AOB21 (bottom) and comparison with ray-theoretic predictions.

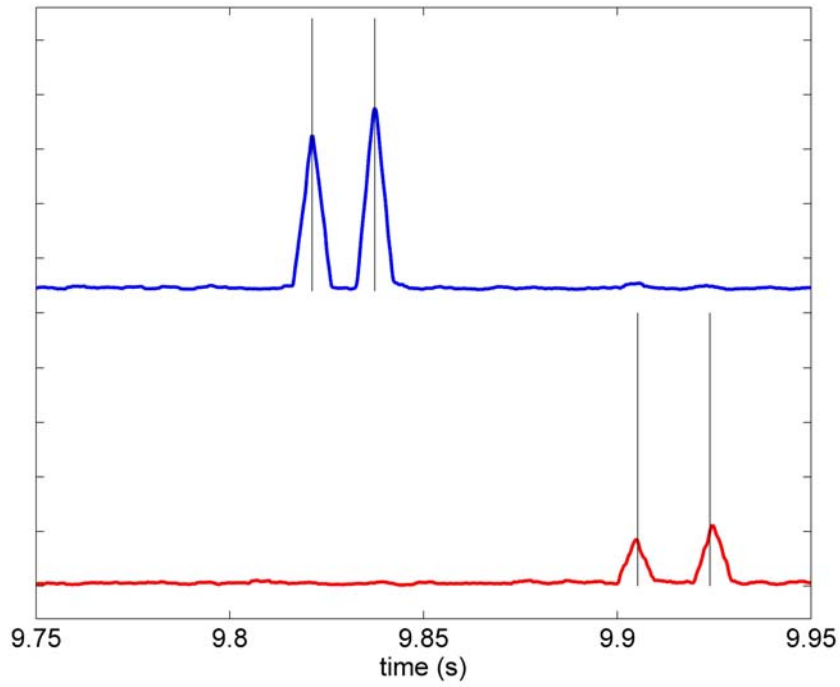


Fig. 3.5.5 Calibration reception (energy-filter output) recorded at AOB22 (top) and AOB21 after offset calibration by 2.97354 sec (bottom) and comparison with ray-theoretic predictions - detail.

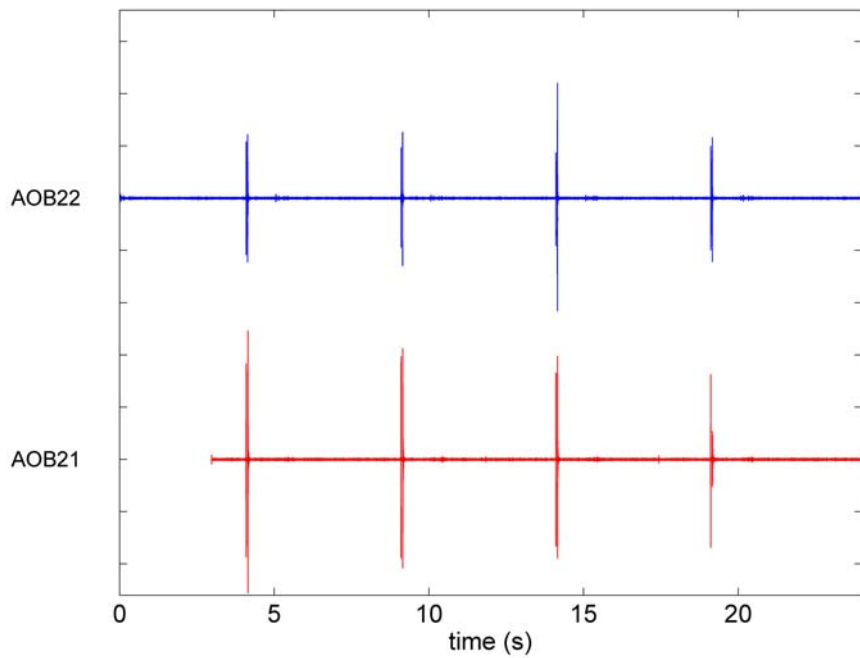


Fig. 3.5.6 Corresponding 24-sec records from AOB22 (top) and AOB21 after offset calibration by 2.97354 sec (bottom) at the beginning of station S1 including control pings for acoustic source.

4. Localization results

In this section the offset-calibrated TOAD data from the lowermost hydrophones of AOB21 and AOB22 are analyzed to obtain information about the source location. The analysis is performed at different levels depending on the amount of data used.

A problem that considerably hampers the localization analysis is the lack of data for the hydrophone depths. As already mentioned these are very important data for the localization and for an accurate localization they should be known at the time of each reception with an accuracy of ~ 0.1 m rms. What we have instead is a rough estimate of the corresponding variability intervals, 75 to 81 m for AOB21 and 64 to 67 m for AOB22. The corresponding nominal depths are 80 and 66.3 m respectively. The upper limits correspond to possible temporary immersion of the buoys e.g. due to waves. The lower limits correspond to a tilt of the suspended arrays caused by drifting of the AOBs.

In subsection 4.1 compatibility checks are carried out based on the TOADs between direct and surface-reflected arrivals at the two AOBs during the stations by comparing the isochrones with the range-depth data from the source depth sensor and the GPS data, where available, taking into account the depth uncertainty of the hydrophones. In subsection 4.2 a first localization analysis is attempted taking into account the depth uncertainty. The results from this analysis are very ambiguous, as expected, because of the large hydrophone depth uncertainty. Finally in subsection 4.3 it is attempted to use part of the verification data, in particular the source depth data from the corresponding depth sensor, in order to constrain the localization analysis. In this way localization results are obtained for the source ranges from the two hydrophones as well as estimates for the hydrophone depths during each station. The results from this analysis are in remarkable agreement with the anticipated intervals for the source ranges, where available.

4.1 Comparison of isochrones with range-depth verification data

A TOAD value between direct and surface-reflected arrival at a certain hydrophone in combination with the hydrophone depth and the sound-speed profile defines the isochrone passing through the range-depth location of the source, cf. section 2. This isochrone can be compared with range-depth data from the source depth sensor and the GPS data, where available. In the case of AOB22 GPS data are available for all stations, whereas for AOB21 such data are available only during the last station S8, cf. Fig. 3.2.3.1. In this connection comparisons can be drawn for AOB21 at station S8 and for AOB22 at stations S1, S2, S4, S7 and S8. In the following, comparisons of isochrones obtained from TOAD data during these stations are presented. In order to account for the hydrophone depth uncertainty the isochrones are calculated assuming two different hydrophone depths, 76 and 78 m for AOB21, 64 and 66 m for AOB22. The results are shown in Figs. 4.1.1-4.1.6. The isochrones corresponding to the shallower/deeper hydrophones depths are marked by the blue/green lines, respectively. In all cases the isochrones pass through the range-depth uncertainty areas (horizontal lines) estimated from the GPS data and source depths, cf. subsection 3.2.3. On the other hand, the isochrones are range-depth loci and do not give a range or depth estimate. As a matter of fact, it is the appropriate intersection of two isochrones that gives the range and depth estimates. From the figures it becomes evident that a slight change in the isochrone can dramatically change the point of intersection.

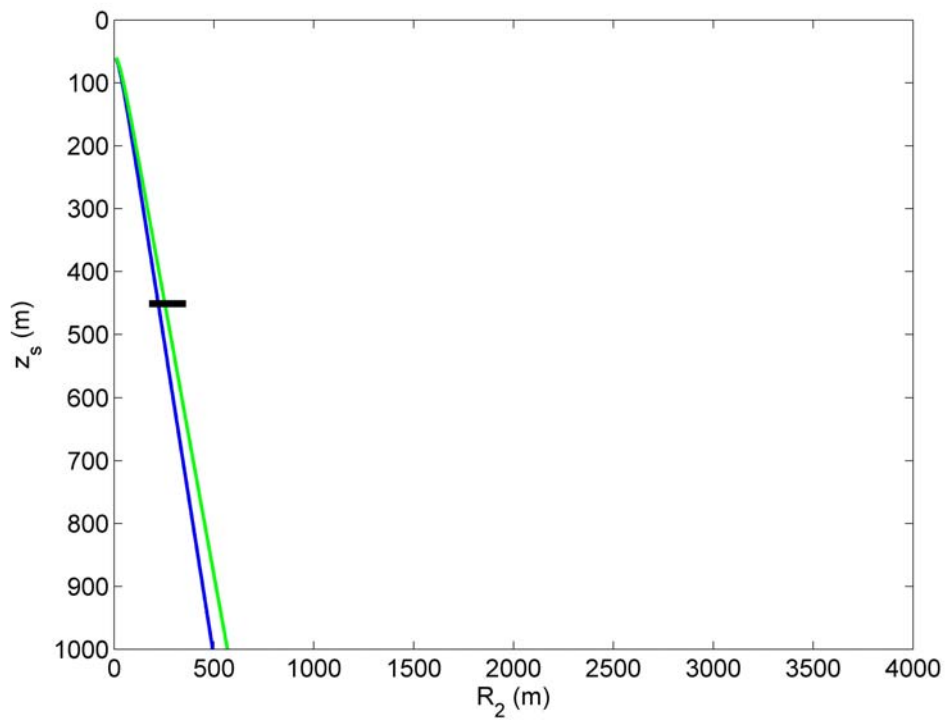


Fig. 4.1.1 Comparison of isochrone corresponding to AOB22 lowermost hydrophone at a depth of 64 m (blue) and 66 m (green) with the source range-depth uncertainty line (black) during station S1.

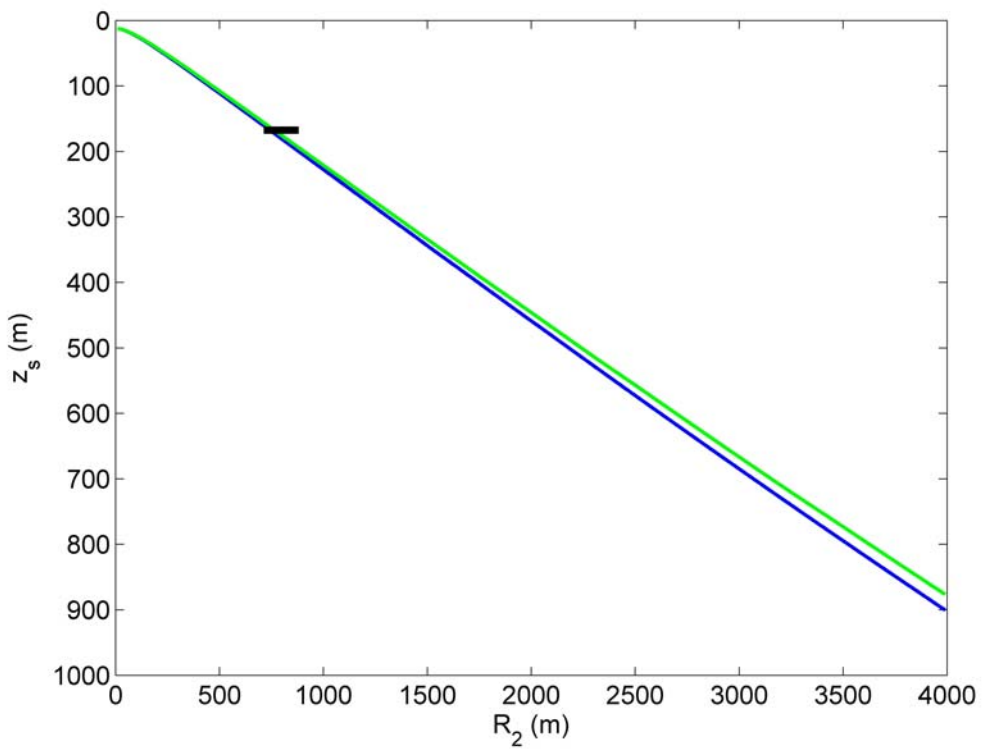


Fig. 4.1.2 Comparison of isochrone corresponding to AOB22 lowermost hydrophone at a depth of 64 m (blue) and 66 m (green) with the source range-depth uncertainty line (black) during station S2.

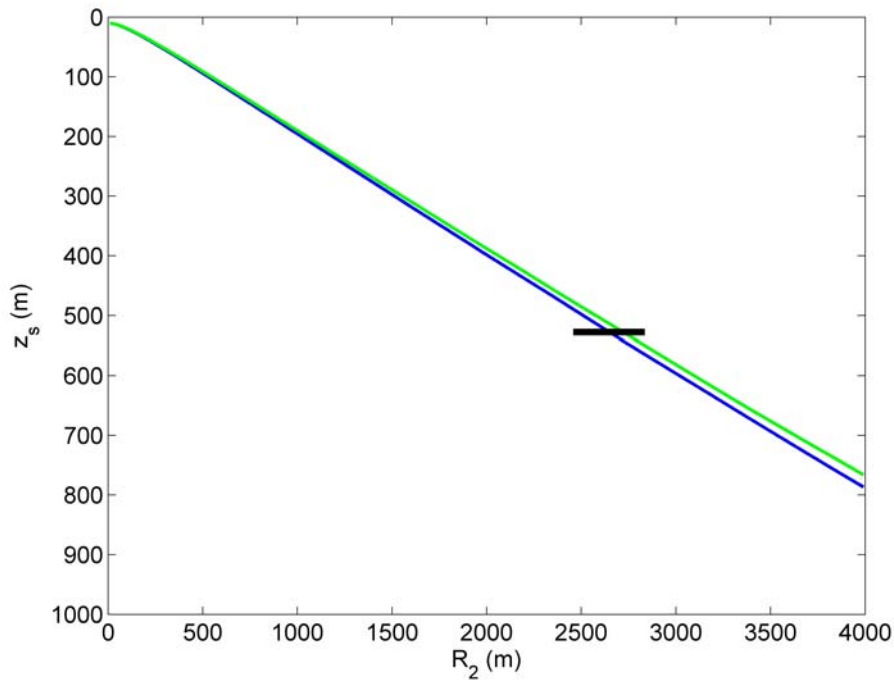


Fig. 4.1.3 Comparison of isochrone corresponding to AOB22 lowermost hydrophone at a depth of 64 m (blue) and 66 m (green) with the source range-depth uncertainty line (black) during station S4.

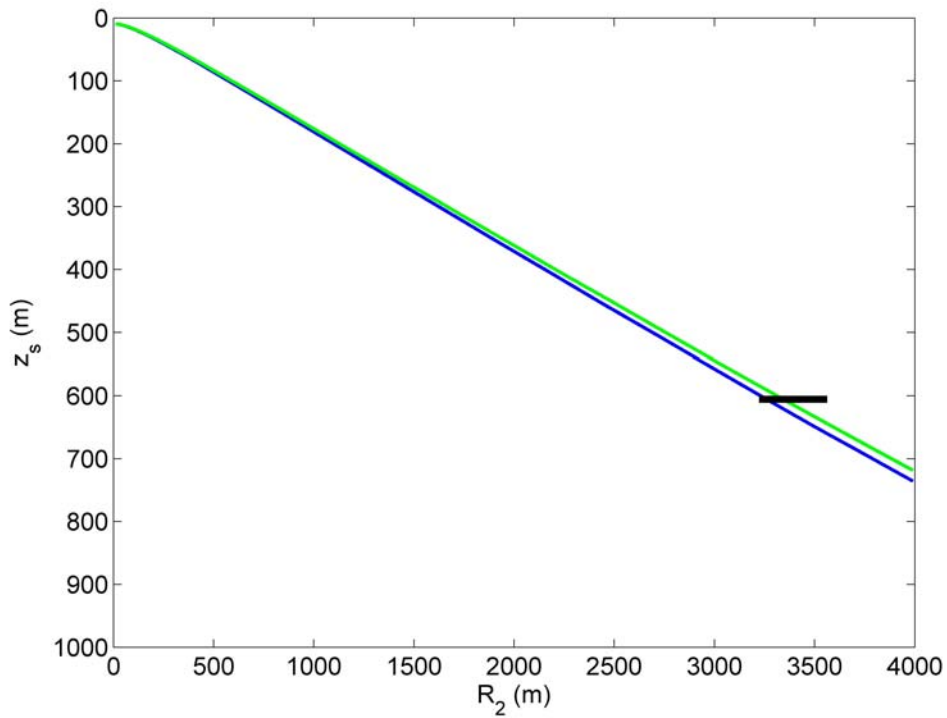


Fig. 4.1.4 Comparison of isochrone corresponding to AOB22 lowermost hydrophone at a depth of 64 m (blue) and 66 m (green) with the source range-depth uncertainty line (black) during station S7.

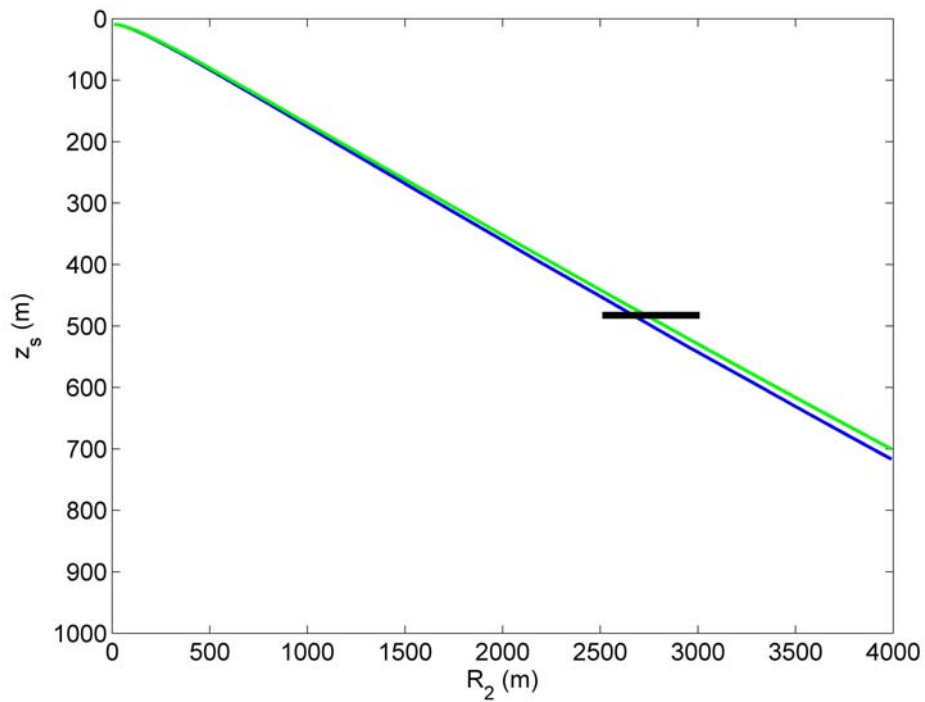


Fig. 4.1.5 Comparison of isochrone corresponding to AOB22 lowermost hydrophone at a depth of 64 m (blue) and 66 m (green) with the source range-depth uncertainty line (black) during station S8.

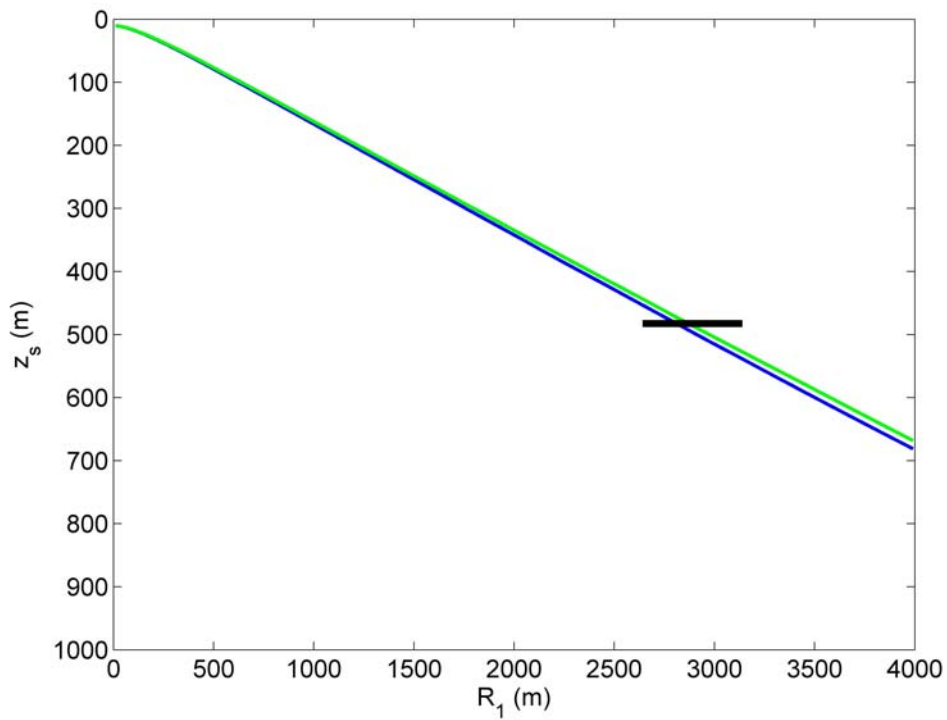


Fig. 4.1.6 Comparison of isochrone corresponding to AOB21 lowermost hydrophone at a depth of 76 m (blue) and 79 m (green) with the source range-depth uncertainty line (black) during station S8.

4.2 Source range and depth estimation – effect of hydrophone depth uncertainty

The sensitivity of source range and depth estimation to changes in hydrophone depths is addressed here. The hydrophone depth uncertainty intervals (75-81 m for AOB21 and 63-67 m for AOB22) are discretized with a step of 0.2 m (31 and 21 points for each interval, respectively) and inversions of the TOAD data are for each combination of hydrophone depths (31x21=651 combinations in total). The results for the source ranges (distance from AOB21, distance from AOB22) and depth are shown in Fig. 4.2.1

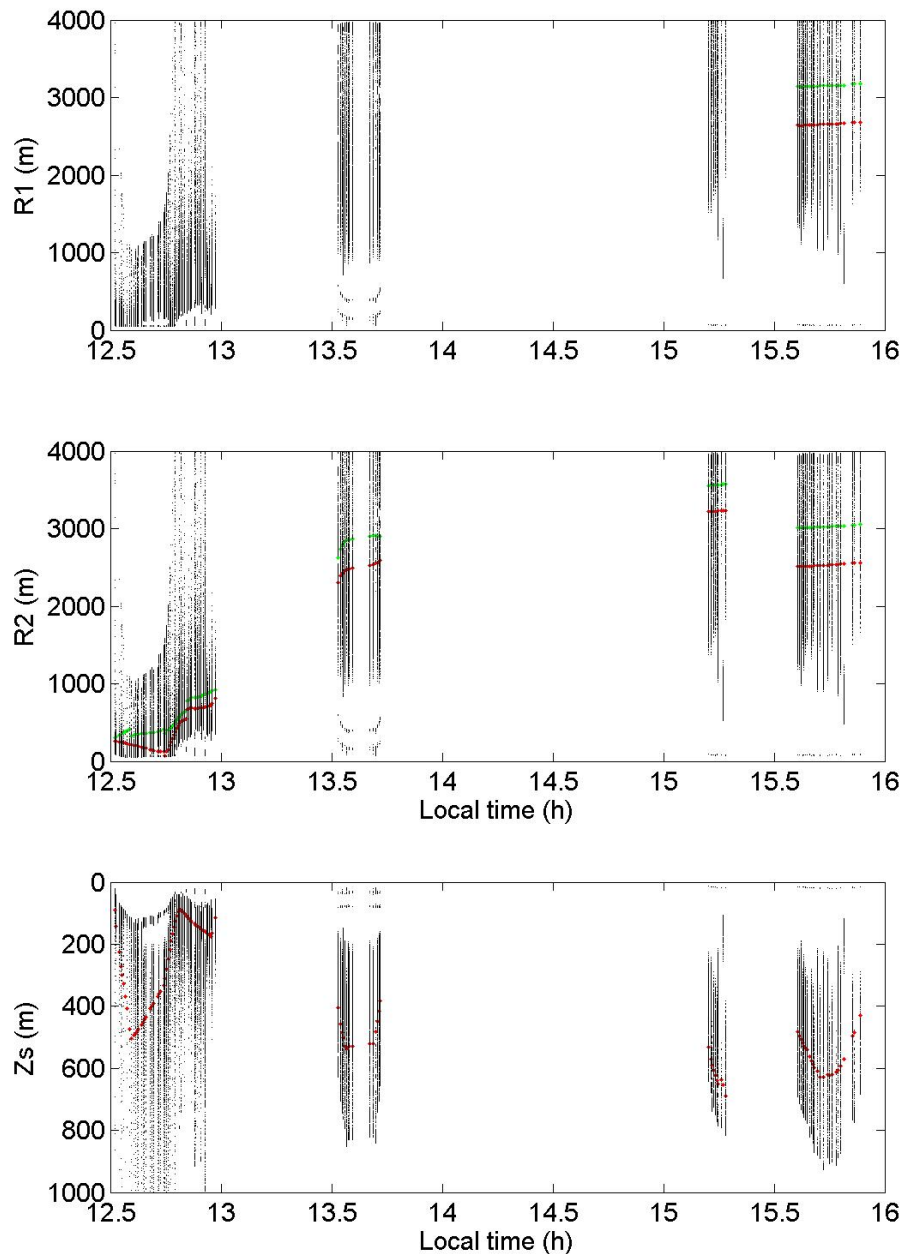


Fig. 4.2.1 Source range and depth estimates (black dots) for all combinations of hydrophone depths in the intervals 75-81 m (AOB21) and 64-67 m (AOB22). Lower and upper range and depth limits from GPS and TDR are shown (red and green dots).

The upper and lower limits for source range and depths based from GPS and TDR are also shown in this figure; in the case of the source depth the two limits practically coincide (the depth accuracy of the TDR is ± 0.5 m). The variability intervals of range and depth estimates from the TOAD inversion include these limits. On the other hand this variability is so big that makes the localization results useless.

4.3 Inversion of TOAD data using source-depth constraint

From the previous results it becomes clear that no useful localization can be carried out if the hydrophone depths are not known with sufficient accuracy. In the given situation, and in order to check localization performance, it is attempted in the following to consider the hydrophone depths as additional to be estimated from the TOAD data. In order to overcome the problem of ill-posedness (multiplicity of solutions) part of the position data, the pinger depth data in particular, is used to constrain the localization analysis.

For the implementation of this approach the hydrophone depth intervals of 75-81 m for AOB21 and 63-67 m for AOB22 are discretized with a step of 0.2 m (31 points for AOB21 hydrophone and 21 points for AOB22 hydrophone, respectively) and inversions of the TOAD data are performed for each combination of hydrophone depths ($31 \times 21 = 651$ combinations in total for each reception). Out of the 651 inversion results for each reception – one reception from each 24-sec record – the combination that gives source depth closest to the measured source depth (from the TDR) at the time of the reception is selected. The source range corresponding to this selection is then the range estimate from the particular reception which is compared with the range estimates from GPS and TDR data.

Fig. 4.3.1 shows the source ranges and depth resulting from this approach. The estimated minimum and maximum ranges based on the GPS and TDR data are also marked (red and green dots, respectively) – GPS data and corresponding range estimates for AOB21 exist only during the last station. While the agreement of source depths is anticipated (since the method seeks to minimize difference between measured and predicted source depths) the agreement between the ranges is remarkable. In most cases the estimated source ranges lie within the anticipated ranges based on the GPS data. Even for the passage from station S1 to S2 where the anticipated range interval is very narrow the localization results fall within the limits. It is reiterated that for the estimation of source ranges and depth the location of the hydrophones in the horizontal is not required. This is fully demonstrated in Fig. 4.3.1: even though we have no position data for AOB21 the horizontal distances of the source from the two hydrophones are estimated and they compare favorably with the verification data where available. Fig. 4.3.2. shows the estimated hydrophone depths. It appears that there is significant variability in the hydrophone depths, with mean values well within the search intervals.

As already mentioned, in order to estimate source depth and horizontal distance from each hydrophone it is not required to know the horizontal location of the hydrophones but merely the hydrophone depths. If in addition the horizontal location of the two hydrophones is known then the source bearing can be estimated as well, subject to left-right ambiguity. The latter is the case only during the last station S8, where the GPS positions of both AOBs are known. The highest accuracy in bearing estimation is obtained when the source is located at the broadside of the two hydrophones; the worst case for bearing estimation is when the source lies close the endfire position [4], [8]. Unfortunately this is the case for station S8.

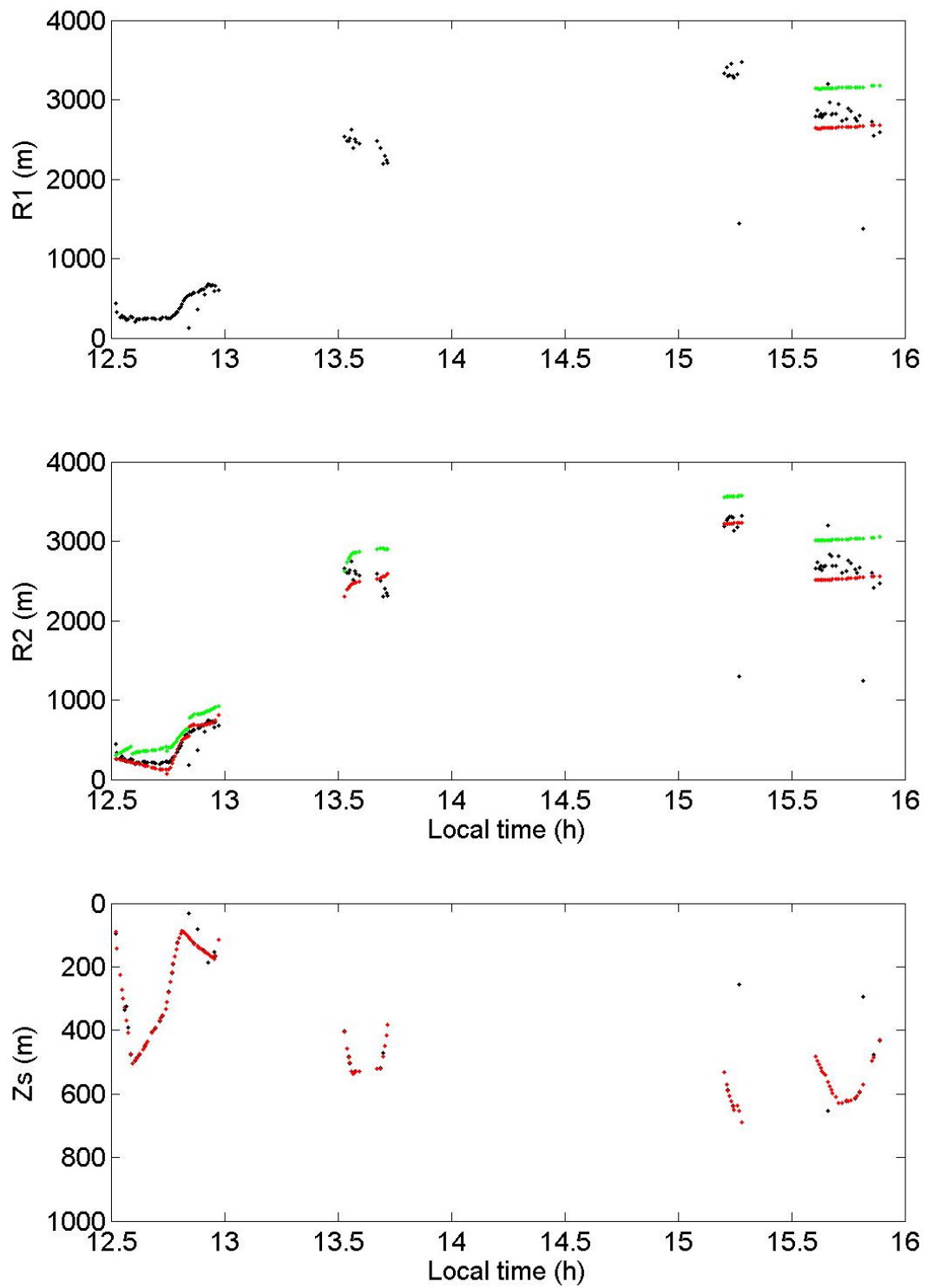


Fig. 4.3.1 Source range and depth estimates constrained by TDR (source depth) data. Lower and upper range and depth limits from GPS and TDR are shown as red and green dots.

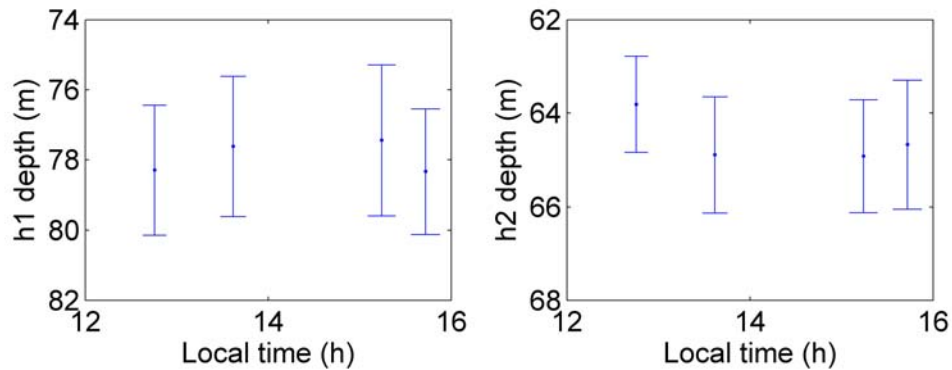


Fig. 4.3.2 Estimated hydrophone depths for the lowermost hydrophone of AOB21 (bottom) and AOB22 (top).

Fig. 4.3.3. shows the estimated location of the source in the horizontal for station S8. The two groups of locations (triangles and circles) in this figure are due to left-right ambiguity. The AOB locations used to obtain these estimates are shown in red for AOB21 and green for AOB22, whereas the corresponding locations of the ship are marked by the blue dots. While the source range falls within the anticipated limits, as seen in Fig. 4.3.1, the source bearing exhibits large variability (about 30°), in agreement with the above remarks. The reason is that the bearing is the result of the intersection of two circles centered at AOB locations. If the intersection is close to the endfire, then the two circles become close to tangent to each other and thus the intersection becomes more and more ambiguous. In other words small errors in range estimation or hydrophone location will cause large errors in bearing estimation. On the other hand, if the intersection lies close to the broadside the bearing estimation is robust, i.e. less sensitive to range estimation errors and distance between the two hydrophones.

In order to illustrate this latter point a bearing estimation for the intermediate station S4 is performed. Since no GPS data are available for AOB21 during that station an assumption is made that AOB21 lies 100 m west / northwest of AOB22 (whose location is known) – AOB21 is shifted to the north to match predicted and observed TOADs between direct arrivals at the two buoys. The results of horizontal localization are shown in Fig. 4.3.4. In this case stable bearing estimates are obtained, which combined with the range estimates indicate that the acoustic source lies between stations S3 and S4 and is moving south. As in the previous figure the AOB21, AOB22 and ship locations used to obtain these estimates are marked by the red, green and blue dots, respectively. During station S4 the source lies behind the ship at a distance between 500 and 800 m, as estimated from the cable length (1000 m) and the depth sensor data (depth of about 500 m). This expectation is in agreement with the results shown in Fig. 4.3.4 and moreover the figure shows a steady southward direction of the source route, which is in agreement with the ship drift during station S8. The symmetric location estimates are not shown since they are outside (west) of the area shown in Fig 4.3.4.

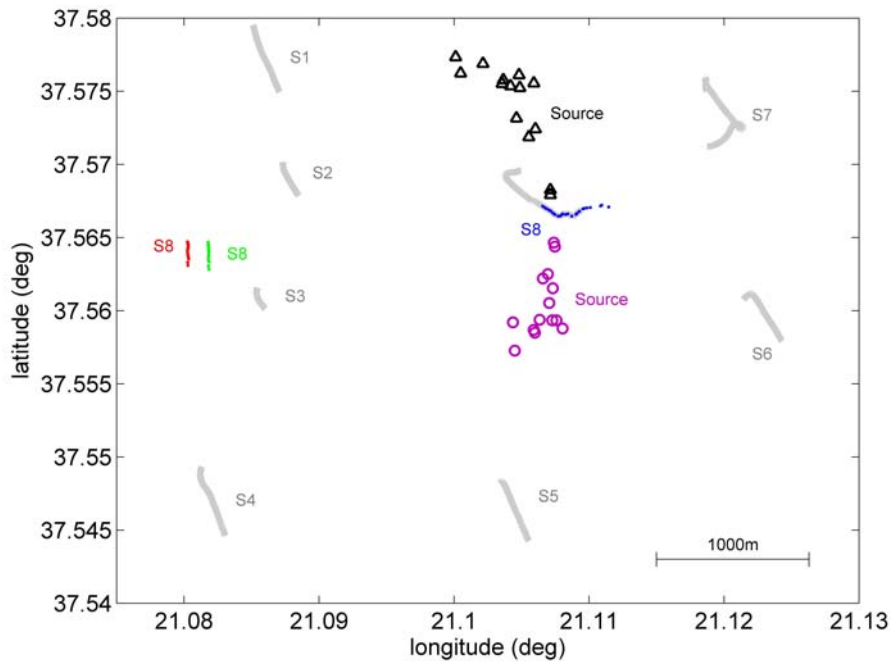


Fig. 4.3.3 Estimated horizontal location of the source (triangles/circles) during station S8. The AOB locations used to obtain these estimates are shown in red for AOB21 and green for AOB22. The grey lines mark the ship locations during stations whereas the blue dots mark the ship locations at the times of bearing estimation.

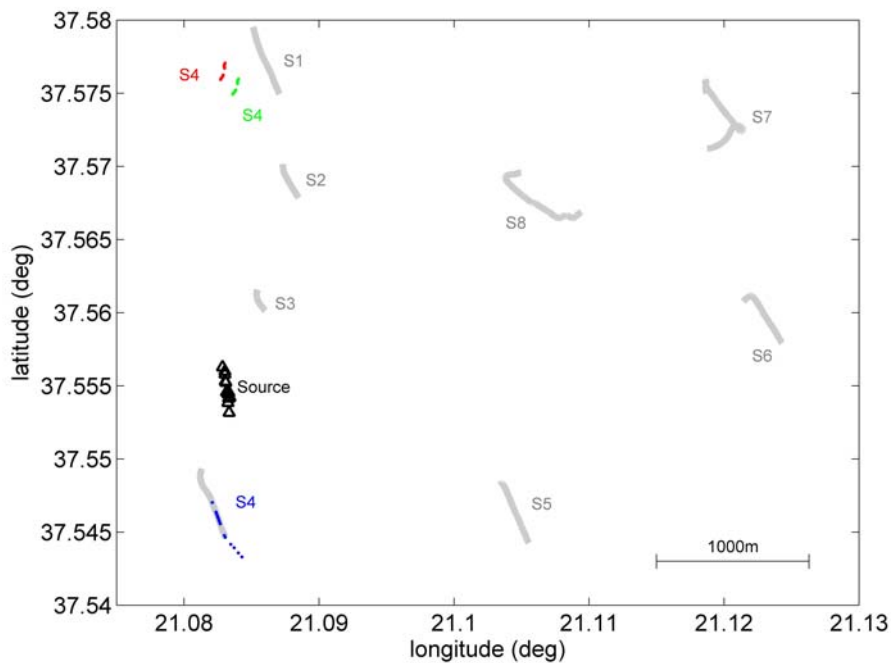


Fig. 4.3.4 Estimated horizontal location of the source (triangles) during station S4, with assumed AOB21 location 100 m northwest of AOB22 (locations in red and green, respectively). The grey lines mark the ship locations during stations whereas the blue dots mark the ship locations at the times of bearing estimation.

5. Discussion and Conclusions

One of the basic Edelweis'14 objectives was to conduct a controlled localization experiment in the Ionian Sea using a pair of hydrophones and a broadband acoustic source deployed at depths compatible with sperm whale diving, in various configurations and setups so as to allow source localization and validation. The localization method exploits time of arrival differences (TOADs) between direct, and also between direct and surface-reflected arrivals at the two hydrophones to obtain estimates for source range, depth and azimuth. For the estimation of source range and depth it is not required to know the horizontal location of the hydrophones but merely the hydrophone depths. If in addition the horizontal location of the two hydrophones is known then the source bearing can be estimated as well, subject to left-right ambiguity.

For the preparation of the controlled localization experiment a preliminary propagation study was conducted taking into account the anticipated propagation conditions in the Ionian Sea in summer and the planned experiment geometry (source-receiver ranges and depths). Two basic goals were to avoid shadow zones for acoustic receptions and no-resolution zones for acoustic TOADs. The two zones were calculated for different source-receiver configurations using ray theory. The obtained results were a great help for decisions made during the experiment, regarding the selection of range and depth combinations which resulted in strong acoustic receptions of both direct and surface-reflected arrivals with sufficient separation. The acoustic data obtained during the experiment fully confirmed those calculations.

The Edelweis'14 controlled localization experiment was conducted with R/V Nereis on 9 August 2014 southeast of Zakynthos island in the Ionian Sea. A limiting factor throughout the Edelweis'14 experiment was the weather. Even though typical weather conditions in the Ionian Sea in summer are mild winds and calm seas, in the case of Edelweis'14 the weather was very variable starting with calm seas in the morning and rapidly deteriorating during noon and afternoon. This greatly affected the implementation of the controlled localization experiment since the deployment and recovery of the AOBs took place by hand. Further, there was significant drift of the ship at a speed ~ 1.2 kn southward. The drift of the AOBs was in about the same direction but slower (~ 0.3 kn).

Further deteriorating factors had to do with shortcomings of the AOBs but also with the dynamic behavior of the acoustic source towed behind R/V Nereis. The problems on the side of the AOBs were the lack of synchronization between the two AOBs, the lack of GPS data for AOB21 for the largest part of the experiment, and the lack of hydrophone depth data. On the side of the acoustic source the major problem was the limited descend of the source during stations. Depending on the ship drift direction the acoustic source never reached depths close to cable length, which would correspond to a vertical cable. During the tow at speeds ~ 4 kn from one station to the next the source ascended to depths as small as 20 m at distances as large as 1 km behind the ship. During stations with drift in the same direction as that of the tow the source hardly sank to depths larger than 200 m. When the drift was to the side of the ship route (stations S5 and S6) the source reached depths of ~ 400 m. Because of this behavior the acoustic source stayed in the shadow/no-resolution zones during stations S3, S5 and S6, and consequently no TOAD data are available at those stations. The largest source depth (~ 700 m) was reached when the drift was opposite to the ship route (station S7).

From the tactical point of view, a problem was the absence of source depth monitoring – the source-depth data became available only after source and TDR recovery. A further tactical factor was the lack of communication between the ship and AOB21, due to which

the orientation of the ship with respect to the AOBs could not be estimated, since the position data of AOB21 were missing.

The initial purpose of the GPS data (location data for the ship and the two AOBs) and the source depth data was for verification and assessment of the localization performance. Part of these data was used in order to solve the above mentioned synchronization problem between the buoys and the lack of data for the hydrophone depths. In particular GPS data from both buoys and the ship during station S8 were combined with source depth data during that station in order to obtain an approximate propagation geometry which was then used in order to conduct model-based predictions of TOADs using the measured temperature and sound-speed data. By comparing predicted and measured TOADs the latter were corrected by introducing a constant time offset in one of the buoys to match predictions (model-based synchronization, offset calibration).

The most hampering factor for the localization analysis of the Edelweis'14 experiment was the lack of data for the hydrophone depths. Hydrophone depths are very important data for the localization and for an accurate localization they should be known with an accuracy of ~ 0.1 m rms. What we know instead is the corresponding variability intervals. While this uncertainty does not appear to pose a problem for the compatibility checks performed in subsection 4.1 – the isochrones pass through the corresponding range-depth uncertainty areas – it does have a large impact when it comes to intersection of isochrones needed for the solution of the localization problem. The resulting errors in range-depth estimation due to the above mentioned uncertainty in hydrophone depths are unacceptable, as shown in subsection 4.2. The situation was improved by using another part of the verification data, those for the source depth, in order to further constrain the localization, practically also invert for the hydrophone depths. This approach worked well and the remaining verification data, those for the estimated source range, compare favorably with the inversion results as shown in subsection 4.3.

With the latter estimates for the source ranges, the horizontal position of the source was estimated for the case of the last station S8, during which GPS data exist for both buoys. Unfortunately during this station the source lies close to the enfire position of the two AOBs for which the bearing errors are largest. This shows in the estimation results: While the ranges are within the expected limits the bearing shows a variability of about 30° . In order to show the dependence of bearing estimation error on source azimuth a bearing estimation was carried out for the intermediate station S4 assuming AOB21 to lie 100 m northwest of AOB22, taking into account the TOADs between direct arrivals at the two hydrophones. Despite the AOB position uncertainty a much clearer picture for the source bearing is obtained, compared to station S8.

In the appendix data and localization results are presented relying on acoustic receptions at shallower hydrophones – hydrophones in the middle of the receiving arrays of the two AOBs. From the preliminary analyses, cf. subsection 3.1.1, it is known that shallower hydrophones are characterized by larger shadow zones as well as larger no-resolution zones, i.e. smaller coverage. This is confirmed by the weaker and lower-quality signals at the shallow hydrophones and the corresponding smaller amount of TOAD data. The localization results from those data are in good agreement with the anticipated ranges.

Based on the above, the following recommendations can be made concerning future steps towards a whale detection, localization and monitoring system

- Hydrophones at depths 60-80 m. Shallower hydrophones may miss data due to shadow zones and/or no-resolution zones.
- Monitoring of hydrophone depths with accuracy 0.1 m rms. Larger errors will greatly deteriorate localization performance
- Hydrophone synchronization and TOAD estimation between direct arrivals at the two hydrophones with accuracy 1 msec or better
- TOAD estimation between direct and surface-reflected arrivals at the same hydrophone with accuracy 0.1 msec or better.
- Possible use of 3-hydrophone triangle-shaped configurations to resolve left-right ambiguity and provide more homogeneous localization accuracy with respect to source azimuth.

6. References

- [1] Frantzis A., Swift R., Gillespie D., Menhennett C., Gordon J. and Gialinakis S., Sperm whale presence off South-West Crete, Greece, Eastern Mediterranean Sea, in European Research on Cetaceans - 13. Proc. 13th Ann. Conf. ECS, Valencia, 20-24 April, 1999, pp. 214-217, 2000.
- [2] Frantzis A., Alexiadou P., Paximadis G., Politi E., Gannier A. and Corsini-Foka M., Current knowledge of the cetacean fauna of the Greek Seas, Journal of Cetacean Research Management, Vol. 5, pp. 219-232, 2003.
- [3] Pesante G., Collet A., Dhermain F., Frantzis A., Panigada S., Podesta M. and Zanardelli M., Review of Collisions in the Mediterranean Sea. Proc. workshop: "Collisions between cetaceans and vessels: can we find solutions?", 6 May 2001, Rome, Italy, ECS newsletter 40 (special issue), pp. 5-12, 2002.
- [4] Frantzis A., Alexiadou P. and Gkikopoulou K.C., Sperm whale occurrence, site fidelity and social organization along the Hellenic Trench (Greece, Mediterranean Sea). Aquatic Conservation: Marine and Freshwater Ecosystems, Vol. 24, pp. 83-102, 2014.
- [5] Taylor, B.L., Baird, R., Barlow, J., Dawson, S.M., Ford, J., Mead, J.G., Notarbartolo di Sciara, G., Wade, P. and Pitman, R.L., *Physeter macrocephalus*, IUCN Red List of Threatened Species, 2008.
- [6] Frantzis A., Airoidi S., Notarbartolo-di-Sciara G., Johnson C. and Mazzariol S., Inter-basin movements of Mediterranean sperm whales provide insight into their population structure and conservation, Deep-Sea Research, Vol. I-58, pp. 454-459, 2011.
- [7] Jesus S.M. and Zabel F., EDELWEIS 2014 Acoustic Oceanographic Buoy Data, Report 02/14 – SiPLAB, 18, October 2014.
- [8] Silva A., Zabel F. and Martins C., Acoustic oceanographic buoy: a telemetry system that meets rapid environmental assessment requirements, Sea Technology, Vol. 47, pp. 15–20, September 2006.

- [9] Skarsoulis E.K., Frantzis A. and Kalogerakis M., Passive localization of pulsed sound sources with a 2-hydrophone array. Proc 7th Eur. Conf. Underwater Acoustics, Delft, The Netherlands, 2004.
- [10] Watkins W.A. and Schevill W.E., Sound source location by arrival times on a non-rigid three-dimensional hydrophone array, Deep-Sea Res, Vol. 19, pp. 691–706, 1972.
- [11] Leaper R., Chappell O. and Gordon J., The development of practical techniques for surveying sperm whale populations acoustically, Rep Int. Whal. Commn., Vol. 42, pp. 549-560, 1992.
- [12] Hastie G.D., Swift R.J., Gordon J.C.D., Slessor G. and Turrell W.R., Sperm whale distribution and seasonal density in the Faroe Shetland Channel, J Cetacean Res. Manage., Vol. 5, pp. 247-252, 2003.
- [13] Thode A. Tracking sperm whale (*Physeter macrocephalus*) dive profiles using a towed passive acoustic array, J. Acoust. Soc. Am., Vol. 116, pp. 245–253, 2004.
- [14] Jensen F.B., Kuperman W.A., Porter M.B. and Schmidt H., Computational Ocean Acoustics, American Institute of Physics, Woodbury, NY, 1994.
- [15] Skarsoulis E.K. and Kalogerakis M., Two-hydrophone localization of a click source in the presence of refraction, Applied Acoustics, Vol. 67, pp. 1202-1212, 2006.
- [16] Skarsoulis E.K. and Kalogerakis M. Ray-theoretic localization of an impulsive source in a stratified ocean using two hydrophones, J. Acoust. Soc. Am., Vol. 118, pp. 2934-2943, 2005.
- [17] Thode A., Three-dimensional passive acoustic tracking of sperm whales (*Physeter macrocephalus*) in ray-refracting environments, J. Acoust. Soc. Am., Vol. 118, pp. 3575-3584, 2005.
- [18] Burdic W.S., Underwater acoustic system analysis, Prentice-Hall, New Jersey, 1984.
- [19] Chen C-T. and Millero F.J., Speed of sound in seawater at high pressures, J. Acoust. Soc. Am., Vol. 62, pp. 1129-1135, 1977.
- [20] Brasseur P., The MED2 hydrographic data base. Lit Rev, Vol. 42, pp. 414–415, 1995.

Appendix A

Localization with shallow hydrophones

In this appendix data and localization results are presented relying on acoustic receptions at the hydrophones in the middle of the receiving arrays of the two AOBs. The nominal depths of these hydrophones are 60 m (AOB21) and 50.3 m (AOB22) respectively. The same problems encountered in the case of the deeper hydrophones, namely lack of synchronization between the two AOBs and lack of data for hydrophone depths, limit the analysis of data from the shallower hydrophones as well. The synchronization problem was addressed in subsection 3.5 with model-based offset calibration and resulted in a time offset correction of 2.97354 sec – addition of 2.97354 sec to AOB21 data. The same offset is used here assuming that all receiving channels in an AOB (all hydrophones in the same array) have a common time reference.

Fig. A.1 shows the time of arrival differences (TOADs) between direct and surface-reflected arrivals at the middle hydrophone of AOB21 during the Edelweis'14 controlled localization experiment. The periods of the 8 stations are denoted by the light grey areas. Similarly, Fig. A.2 shows the time of arrival differences between direct and surface-reflected arrivals at the middle hydrophone of AOB22. Finally, Fig. A.3 shows the offset-calibrated TOADs between direct arrivals at the middle hydrophones of AOB21 and AOB22 (time of arrival at AOB22 minus time of arrival at AOB21 – positive means that the signal arrives at AOB21 first, i.e. source closer to AOB21). As in the case of the lowermost hydrophones data are shown only for the cases where full TOAD sets (three TOADs) are available. As explained in subsection 3.3.3 this is the case only during stations S1, S2, S4, S7 and S8 – during stations S3, S5 and S6 there are no TOAD data due to unfavourable source range and depth combinations.

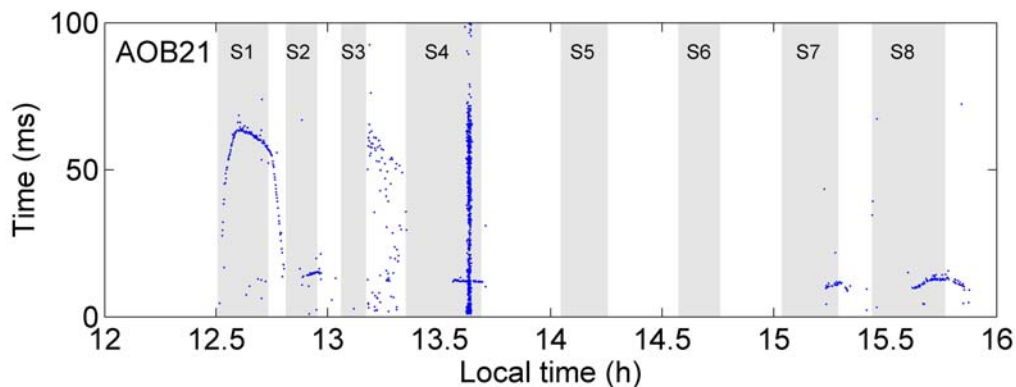


Fig. A.1 Time of arrival differences between direct and surface-reflected arrivals at the middle hydrophone of AOB21. The light grey areas mark the 8 stations.

The TOAD data from the middle hydrophones exhibit a similar picture as in the case of the lowermost hydrophones, presented in subsections 3.3.3 and 3.3.4, still they are less and of lower quality. The reason is that the shallower hydrophones lead to larger/deeper shadow and no-resolution zones, cf. figures in subsection 3.1.1, leaving more source locations uncovered (in comparison to deeper hydrophones). Fig. A4 shows a comparison of receptions at the middle and lowermost hydrophones of AOB22 during

station S7, the same reception as in Fig. 3.3.2.2. The panel on the left shows the frequency-filtered signal and the panel on the right the frequency- and energy-filtered signal. The receptions at the two hydrophones are stacked; the lower one refers to the lowermost hydrophone (66.3 m nominal depth) and the upper one to the middle hydrophone (50.3 m nominal depth). The decrease of acoustic intensity is evident in the reception at the middle hydrophone even though the depth difference is only 16 m; this means lower SNR, poorer detection and arrival time estimation, and finally lower-quality TOAD data at the shallower hydrophone. In conclusion, the deeper the hydrophone the better. With shallow hydrophones acoustic signals can be detected and direct from surface-reflected arrivals separated only if the source is sufficiently deep, depending on range. This can be verified by comparing Figs. A1-3 with Figs. 3.3.3.1-2 and 3.3.4.1, respectively. During the move from station S1 to S2 where the source approaches the surface TOADs are recorded at the lowermost hydrophones but not at the middle hydrophones. Similarly, during stations S4, S7 and S8 the data at the middle hydrophones are less and of lower quality than those at the lowermost hydrophones due to extended shadow/no-resolution zones.

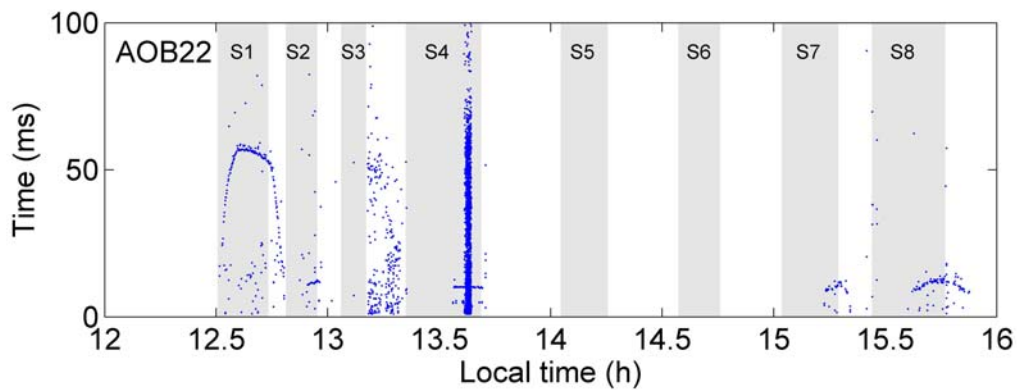


Fig. A.2 Time of arrival differences between direct and surface-reflected arrivals at the middle hydrophone of AOB22. The light grey areas mark the 8 stations.

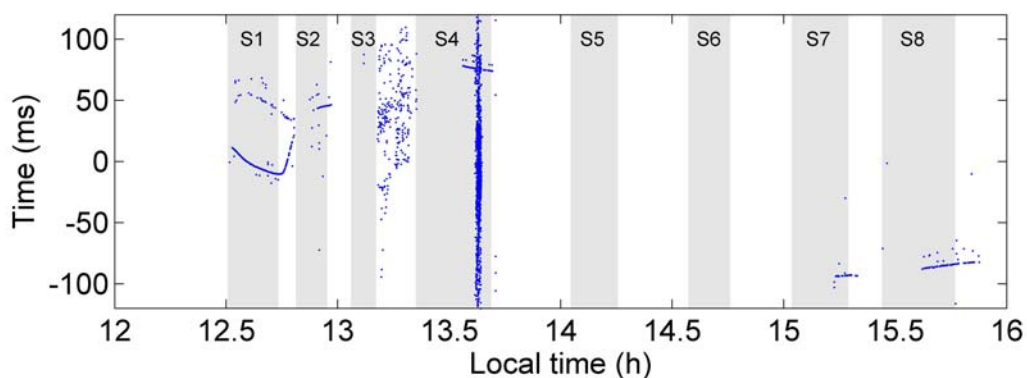


Fig. A.3 Time of arrival differences between direct arrivals at the middle hydrophone of AOB21 and AOB22 (positive means that signal arrives at AOB21 first). The light grey areas mark the 8 stations.

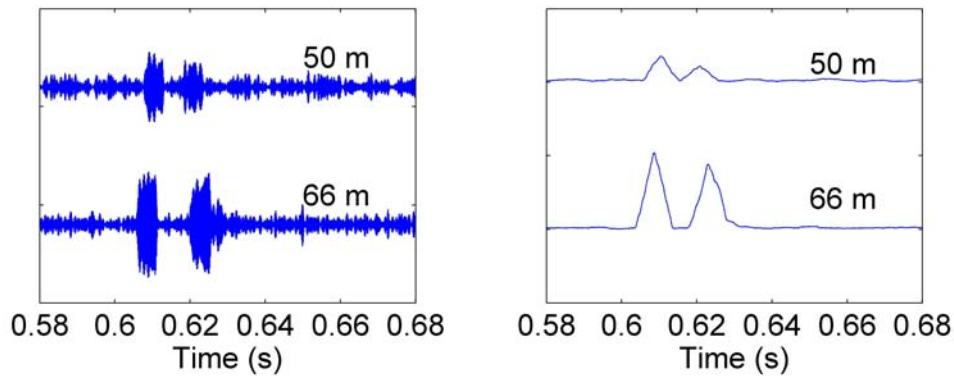


Fig. A.4 Reception during station S7 picked up by the middle (50 m - top) and lowermost (66 m - bottom) hydrophone of AOB22. Left: frequency filtered reception. Right: frequency and energy filtered receptions.

In the following localization results are presented, based on receptions at the middle hydrophones. As in the case of the lowermost hydrophones a major problem in the localization analysis is the lack of data for the hydrophone depths. This is demonstrated in Fig. A.5 which shows estimated source ranges and depth assuming variability intervals of 56-61 m for AOB21 hydrophone and 45-51 m for AOB22 hydrophone, taking into account possible tilt and immersion of the arrays. These intervals are discretized with a step of 0.2 m and all possible depth combinations of the two hydrophones are considered. As in the case of the lowermost hydrophones, Fig. 4.2.1, in Fig. A.5 the localization errors caused by the hydrophone depth uncertainty are extremely large and the results are unacceptable. The message is clear: efficient localization can only be carried out if the hydrophone depths are known to sufficient accuracy.

In the following the hydrophone depths are considered as unknowns of the problem to be estimated from the TOAD and source depth data. The variability intervals – 56-61 m for AOB21 and 47-51 m for AOB22 – are discretized with a step of 0.2 m (26 points for AOB21 hydrophone and 21 points for AOB22 hydrophone, respectively) and inversions of the TOAD data are performed for each combination of hydrophone depths (26x21=546 combinations in total for each reception). Fig. A.6 shows the resulting source ranges and depth. The agreement with the anticipated ranges is good, as in the case of the lowermost hydrophones, apart from the fact that there are fewer points due to the smaller spatial coverage.

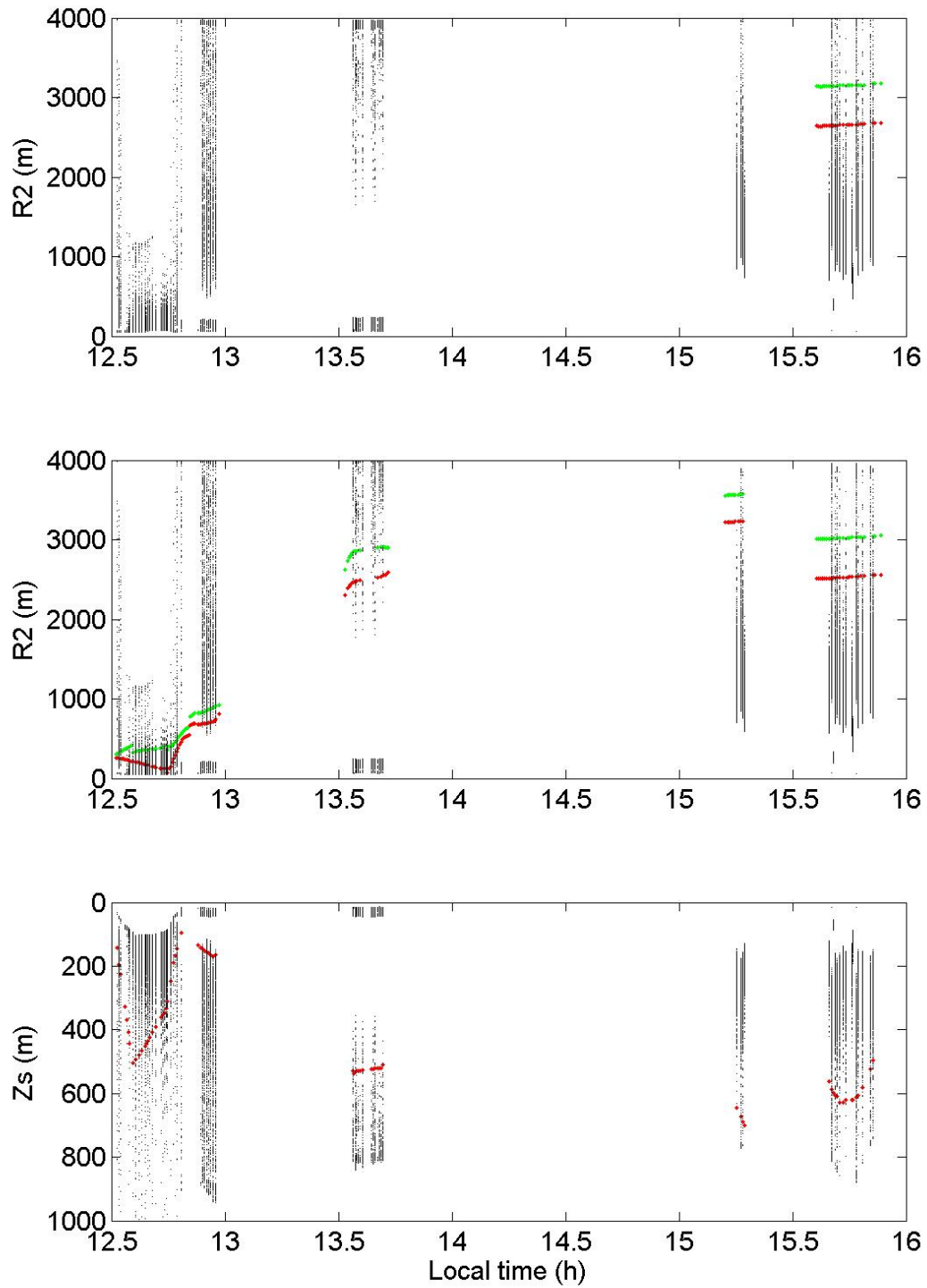


Fig. A.5 Source range and depth estimates for all combinations of hydrophone depths in the intervals 56-61 m (AOB21) and 47-51 m (AOB22) - middle hydrophones. Solid lines indicate lower and upper uncertainty limits for source ranges and depth based on GPS and depth data.

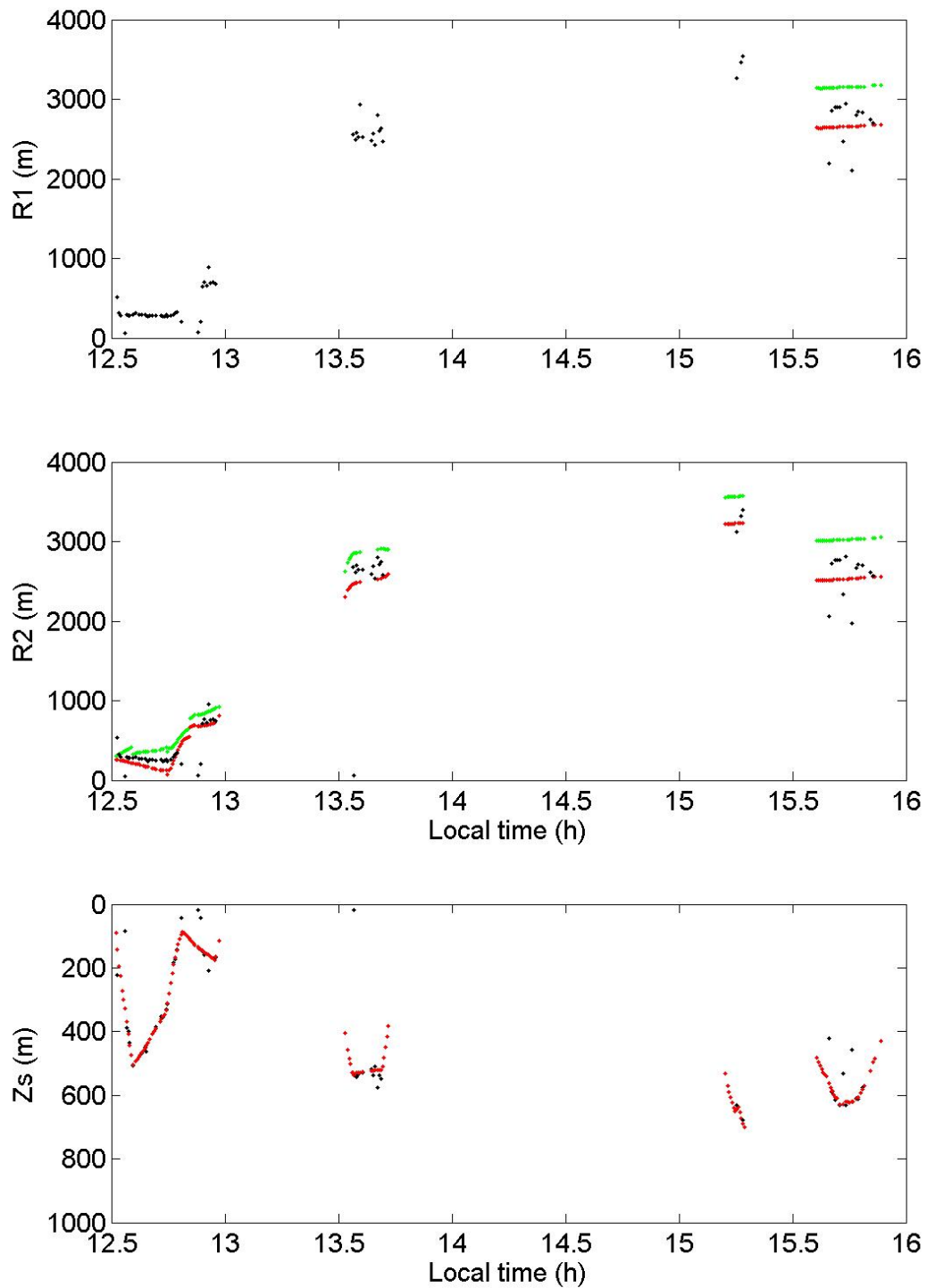


Fig. A.6 Source range and depth estimates from TOADs at the middle hydrophones constrained by source depth data. Solid lines indicate lower and upper uncertainty limits for source ranges and depth based on GPS and depth data.